GEOCHEMISTRY, STRUCTURE, AND TECTONIC EVOLUTION OF THE ELDIVAN OPHIOLITE, ANKARA MÉLANGE, CENTRAL TURKEY

by

Anne Dangerfield

A thesis submitted to the faculty of

Brigham Young University

in partial fulfillment of the requirement for the degree of

Master of Science

Department of Geological Sciences

Brigham Young University

August 2008

BRIGHAM YOUNG UNIVERSITY

GRADUATE COMMITTEE APPROVAL

of a thesis submitted by

Anne Dangerfield

This thesis has been read by each member of the following graduate committee and by majority vote has been found to be satisfactory.

Date	Ronald A. Harris, Chair
Date	Michael J. Dorais
Date	Stephen T. Nelson

BRIGHAM YOUNG UNIVERSITY

As chair of the candidate's graduate committee, I have read the thesis of Anne Dangerfield in its final form and have found that (1) its format, citations, and bibliographical style are consistent and acceptable and fulfill university and department style requirements; (2) its illustrative materials including figures, tables, and charts are in place; and (3) the final manuscript is satisfactory to the graduate committee and is ready for submission to the university library.

Date	Ron A. Harris Chair, Graduate Committee

Accepted for the Department

Date	Scott Ritter Department Chair

Accepted for the College

Date	Thomas W. Sederberg Associate Dean, College of Physical and Mathematical Sciences

ABSTRACT

The Eldivan ophiolite, in the Ankara Mélange, represents the remnant of an ocean basin that developed in the İzmir-Ankara-Erzincan Ocean and collapsed the form the İzmir - Ankara-Erzincan suture zone (İAESZ) through continental block collision. Whole-rock and mineral geochemical evidence show supra-subduction zone tectonomagmatic affinity for the ophiolite, revealing this basin formed in the upper plate of an intra-oceanic subduction zone. Detrital zircon from the ophiolitic mélange sandstone and the overlying Karadağ Formation suggest the ophiolites maximum age is 143.2 (±2) Ma, and the overlying Karadağ Formation is 105.2 (±5) Ma. The angular unconformity between the ophiolite and Karadağ formation reveal that the Eldivan ophiolite was imbricated between 105.2 (±5) Ma and 143.2 (±2) Ma. Petrographic analysis of sandstone from the ophiolitic mélange reveals a source terrain of a volcanic arc rather than a continental source. Structural restoration of the sheeted dike complex reveals the back or intra-arc spreading ridge of the Eldivan ophiolite as NE-SW, oblique to the Sakarya-Pontide continental margin. Three phases of evolution for the Eldivan ophiolite are constrained by complied age data: a constructional, destructional, and suturing phase. The evolution is similar the Philippine Sea Plate and Mariana Trough and fits well within the framework of other eastern Mediterranean Tethyan ophiolites

ACKNOWLEDGMENTS

I would like to thank the American Association of Petroleum Geologists and the National Science Foundation (grant EAR 0337221) for funding this project. Ron Harris provided invaluable support through the entire process, without which this project would not have been completed. Special thanks and appreciation goes to the Maden Tetkik ve Arama Genel Müdürlüğü (MTA) in Turkey and especially Ender Sarıfakıoğlu, Mustafa Sevin, Esra Esirtgen, and Serdal Alemdar for their tremendous help and guidance in the field. Yildirim Dilek provided significant logistical support in initiating the project. I would also like to thank Stephen Nelson and Michael Dorais for critical manuscript reviews and David Tingey for help with analytical equipment and procedures.

TABLE OF CONTENTS

LIST OF FIGURES AND TABLES

INTRODUCTION

Suture zones are present on the majority of the world's continents and represent significant collisional tectonic boundaries between terrains of different affinity and reflect continental development. They represent the only remains of ocean basins that once existed between continents or continental fragments and their tectonic history is a key to understand the formation of continents. Despite their importance, their processes of formation are complex and therefore poorly understood. This study uses the İzmir-Ankara-Erzincan suture zone in Turkey to better understand the tectonics of the eastern Mediterranean region and overall developmental processes that create suture zones.

The İzmir-Ankara-Erzincan suture zone (İAESZ), located in northern Turkey, is a remnant of the Izmir-Ankara- Erzincan ocean (İAEO) branch of the Neo-Tethys that formed during collision of Gondwana derived micro-continents (Kırşehir block and Tauride-Anatolide platform) with the Sakarya-Pontide terrain of northern Turkey (Şengor and Yılmaz, 1981) (Fig. 1a&b). The suture zone is made up of ophiolitic mélange, and includes the Ankara Mélange, located in the center of the suture zone between the Kırşehir block and Sakarya-Pontide terrain.

The Ankara Mélange was first named by Bailey and McCallien (1950) and consists of three major tectonic units. From top to bottom these units are: 1) a metamorphic block mélange, also called the Karakaya Formation (Koçyiğit , 1991) and Karakaya Group (Floyd, 1993); 2) a limestone block mélange; and 3) and ophiolitic mélange (Norman, 1984; Koçyiğit , 1991; Tüysüz et al., 1995; Dilek and Thy, 2006). The tectonically lowest ophiolitic mélange unit consists of blocks of basaltic and rhyolitic volcanic rocks, pillow basalt, serpentinized peridotite and ultramafic rocks, radiolarian

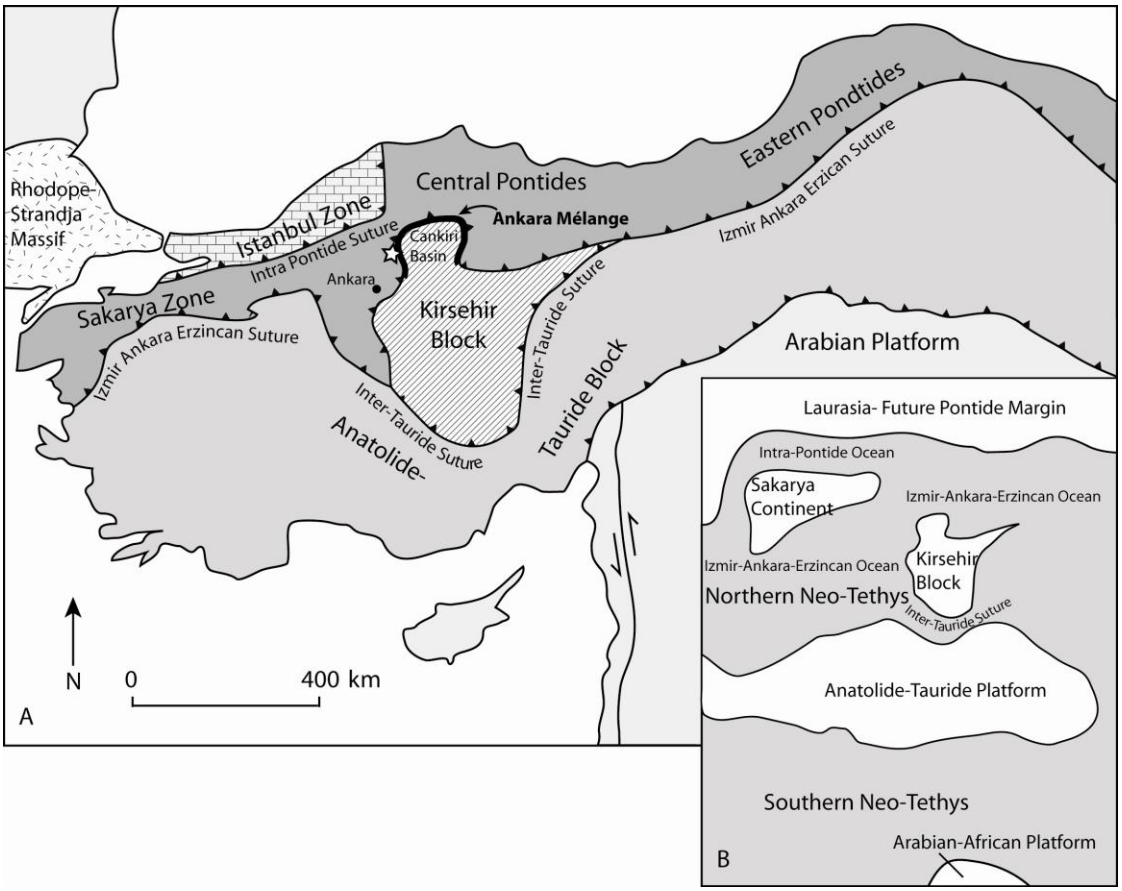

Figure 1. a) Map of the major tectonic units discussed in this paper (after Okay and Tüysüz, 1999). The star is the location of the Eldivan ophiolite and the study area of this paper. b) Reconstruction of the İzmir -Ankara-Erzincan suture zone (after Şengor and Yılmaz, 1981) showing the relationship between ocean branches and continental blocks discussed in this paper.

bearing limestone and chert, with minor shale and sandstone in a serpentinite or tuffaceous matrix (Norman, 1984; Tankut et al., 1998). Dike complexes, where present, are commonly doleritic, cut sequences of serpentinized peridotite and isotropic gabbro, and include plagiogranite (Dilek and Thy, 2006). During convergence, the İAEO crust was imbricated along northward dipping thrust faults (Şengor and Yılmaz, 1981) and overlain by flyschoidal (Norman, 1984) and forearc basin (Koçyiğit, 1991) deposits that were subsequently imbricated with the İAEO crust during the collision of the Kırşehir block and Sakarya-Pontide continent.

Despite previous studies of the Ankara Mélange, its age, origin of formation, and evolutionary history are still poorly understood which, hindering efforts to reconstruct its role in the tectonic evolution of the İAESZ. This study uses crustal and mantle geochemistry, mineral chemistry, petrography, detrital zircon, and structural data from the Eldivan ophiolite in the western Ankara Mélange to create a model for formation of the Ankara Mélange and the tectonic evolution of the central İzmir-Ankara-Erzincan Ocean.

GEOLOGY AND HISTORY OF THE İAESZ

The İAEO opened in the Triassic as a MORB-type oceanic setting based on geochemical results from basalt and associated Triassic radiolarian limestone found along the İAESZ (Tankut, 1984; Tankut et al., 1998; Floyd et al., 2000; Göncüoğlu et al., 2006). Jurassic and Cretaceous alkali basalt is also found in the İAESZ, but is interpreted as seamount fragments accreted to an accretionary wedge (Tüysüz et al., 1995; Floyd et al., 2000; Rojay et al., 2001; Göncüoğlu et al., 2006), possibly in the form of hot-spot generated volcanic ridge systems, (Floyd, 1993; Tankut et al., 1998). Also documented

along the suture are island arc tholeiites (Göncüoğlu et al., 2006; Sarıfakıoğlu, 2006) and calc-alkaline volcanics (Tankut, 1984; Tüysüz et al., 1995; Göncüoğlu et al., 2006), suggesting subduction-related magmatism. Western and central portions of the suture zone have supra-subduction zone (SSZ) basalt, indicating intra-oceanic subduction with upper plate extension (Yalınız et al., 1996; Floyd et al., 1998; Floyd et al., 2000; Yalınız et al., 2000b; Dilek and Thy, 2006; Sarıfakıoğlu, 2006; Sarıfakıoğlu et al., in press). This SSZ signature is similar to other Cretaceous eastern Mediterranean ophiolites (i.e. Pindos, Troodos, Antalya, Hatay (Kızıldag), Baer-Bassit and Semail) and has led to correlations of the İAESZ with the Vardar suture in Greece (Yalınız et al., 2000b; Göncüoğlu et al., 2006, Sarıfakıoğlu et al., in press).

The age of the ocean basin is poorly constrained, particularly the transition between rifting and subduction that lead to closure of the basin. The oldest ages from the basin come from Carnian (Tekin et al., 2002) and Norian (Bragin and Tekin, 1996) radiolaria in limestone and chert blocks that indicate the ocean was open by the Late Triassic period. Post-collisional granitoids ages in the Kırşehir block suggest that continental collision began in the Late Cretaceous period (Boztuğ et al., 2007), finally closing the ocean basin. The transition from rift consturction to subduction closure has been interpreted to have begun as early as 179 Ma (Dilek and Thy, 2006) and as late ~82 Ma (Göncüoğlu et al., 2006). Thus, although the general range of construction of the İAEO (Late Triassic to Late Cretaceous) is established, individual events of its geodynamic history are poorly constrained.

ELDIVAN OPHIOLITIC UNITS

The Eldivan ophiolite forms part of the İAESZ located on the western side of the Ankara Mélange south of the city of Eldivan (Fig. 1). Here, the Eldivan ophiolite is dismembered and exists as imbricated fragments of ophiolitic components (Fig. 2).

The area is dominated by oceanic material with very little continental input. Ophiolitic units present are serpentinized mantle peridotite, massive gabbro, sheeted dikes, pillow basalt and sheet flows, and epi-ophiolitic limestone and chert. Overlying this imbricated ophiolitic mélange is the younger Karadağ Formation, composed of radiolarian bearing pelagic limestone and chert.

Peridotite

Serpentinized peridotite is found in two main locations and is largely diapiric. Small coherent blocks of less altered ultramafic rocks are found within diapiric serpentine, which intrudes vertically into overlying units and along fault planes. The serpentinized peridotite is the matrix for the mélange and contains blocks of basalt, silicic volcanic rocks, limestone, chert, and gabbro. Blocks range in size from a few meters to hundreds of meters, basalt blocks being the largest found. Much of the serpentinite matrix exhibits a scaly shear fabric with anastomosing slicken-sides.

Compositionally, non-diapiric peridotite is spinel-bearing with 95-100% serpentinization. Serpentinized olivine (80-90%) is surrounded by secondary magnetite. Pyroxene (5-10%) has been converted completely to serpentine but still displays the low birefringence and parallel extinction of fresh orthopyroxene crystals. Primary chromian spinel is also found (2-5%).

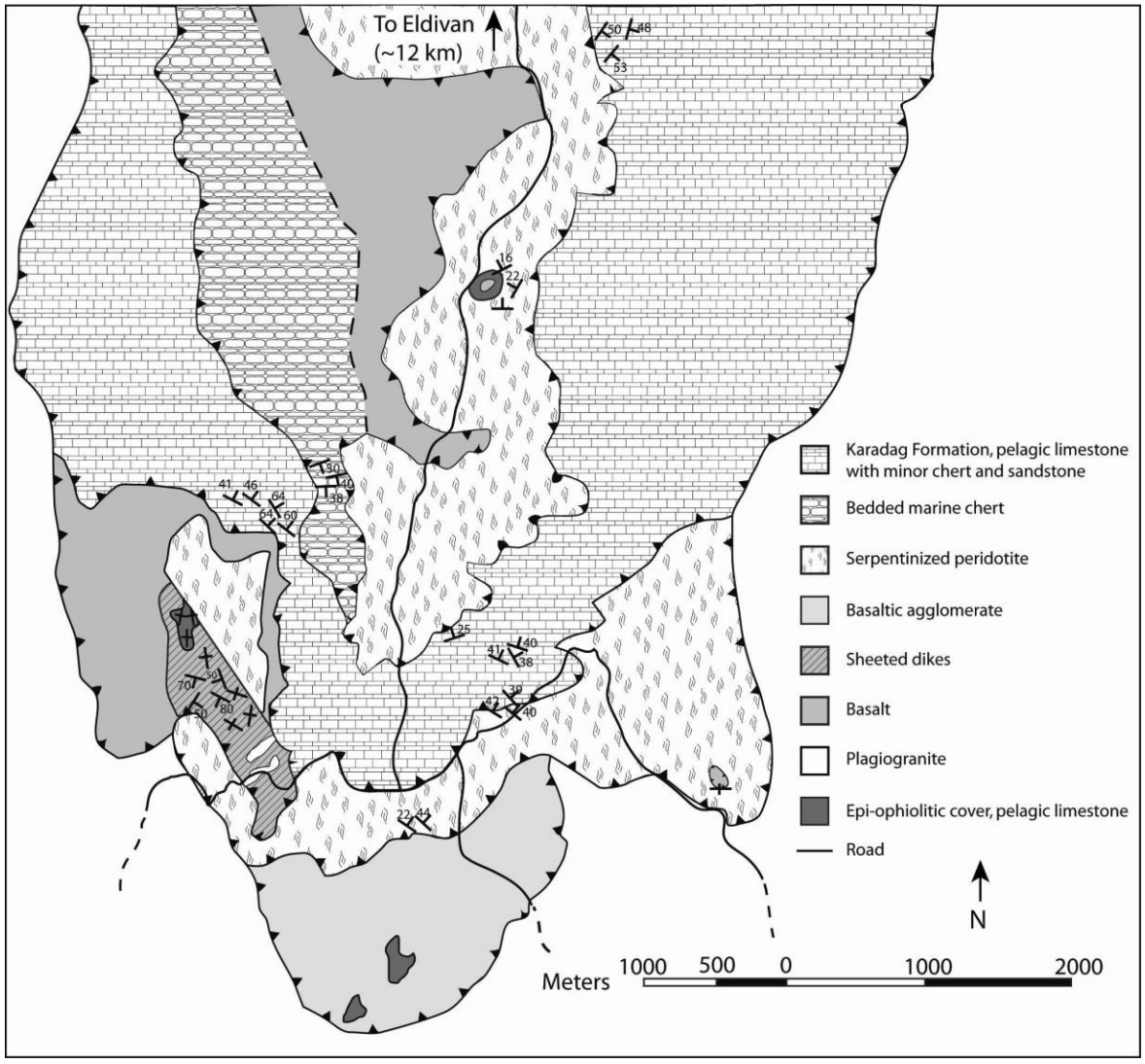

Figure 2. Geologic map of the Çankırı H30-b2 quadrangle (1:25,000). See star in Figure 1 for location.

Massive Gabbro

Massive gabbro occurs in screens within sheeted dikes and is intruded by plagiogranite. Plagiogranite bodies lack chilled margins, tentatively suggesting they could be an immiscible liquid phase within a gabbroic magma chamber or intrusions into a hot un-solidified magma chamber.

Gabbro contains 50% plagioclase (albitized) and 30%-50% clinopyroxene. Rocks show typical greenschist facies hydrothermal metamorphism with actinolite, chlorite, and epidote being common replacement minerals for clinopyroxene and plagioclase. Fe-Ti oxides, most composed of secondary magnetite, make up about 5%.

Sheeted dikes

Sheeted diabase dikes are altered and cut the through massive gabbro screens. Many show chilled margins and some preserve flow fabrics. Fractures and small faults within the dikes have gouge zones filled with epidote and chlorite, which are common seafloor hydrothermal alteration minerals indicating the fractures probably formed during seafloor formation. Dikes show two primary orientations, NNW-SSE and E-W with dips from 40 to 90 degrees. In one locality, the sheeted dikes feed pillow basalts and sheet flows that have been turned vertically, indicating the dikes and basaltic rocks have been rotated from their original position.

Volcanic Sequence

The volcanic sequence includes both basaltic and rhyolitic volcanics as blocks within the serpentinized matrix or whole thrust sheets. Silicic rocks are usually blocks on

the meter to decimeter scale. Basalt occurs as pillows, sheet flows and massive blocks up to tens of square meters in area.

Epi-ophiolitic sediments

Epi-ophiolitic sediment is generally meter to decimeter sized blocks of pelagic, radiolarian bearing limestone and chert within the serpentinized matrix of the mélange but not in direct contact with ophiolitic units. In some cases limestone and chert are intercalated within pillow basalt lobes or in depositional contact with pillow basalts or sheet flows.

Karadağ Formation

The Karadağ Formation, present throughout the Ankara Mélange, is made up of intercalated volcanic and coarse siliciclastics at its base that grade upward into intercalated finer sandstones and mudstones and finally clay rich limestone (Akyurek et al., 1980; Hakyemez et al., 1986). It represents flycsh deposited on the ocean floor, most likely in a fore deep setting near the continental margin that developed as continuing subduction brought continental convergence. The Kursunluduz Member of the Karadağ Formation contains chert bands alternating with red pelagic limestone (Akyurek et al., 1980; Hakyemez et al., 1986). The presence of *Praegglobotruncana stephani*, *Rotaliapora apenninica, Hedbergella* sp., *Ticinella* sp., *Globigerina* sp., Textulariella sp., *Cuneolina* sp., and *Valvulammina* sp. radiolaria suggest the age of the Karadağ is Cenomanian to Campanian in age (Akyurek et al., 1980).

Near the Eldivan ophiolite, the Karadağ Formation is made up of pelagic limestone and chert, sometimes interbedded, with no volcanic material and very little clastic material. An angular unconformity exists between the Karadağ formation and the

underlying imbricated ophiolitic material in the Ankara Mélange. This suggests that, in some areas, the Karadağ formation was deposited after or during the imbrication of the ophiolite, and is in part correlative to the overlying Maastrichtian flycsh of Norman (1984).

WHOLE-ROCK AND MINERAL GEOCHEMISTRY

Serpentinized peridotite, volcanic rocks, diabase dikes, and gabbro were analyzed for whole rock major, trace, and rare-earth elements (REE) and mineral chemistry. Major and selected trace element x-ray florescence (XRF) analysis was conducted at Brigham Young University. Trace and rare earth elements were analyzed by ICP-MS at ALS Chemex laboratories Vancouver, British Columbia (method ME-MS81). Mineral chemistry analysis was conducted using a Cameca SX-50 Electron Microprobe at Brigham Young University. Results of analyses are given in tables A1 and A2. Due to the high degree of alteration indicated by widespread secondary mineralization, most of it hydrous, and resulting elevated LOI values (up to 5% for mafic rocks and 12% for ultramafic), calcined samples were used for analyses, and only relatively immobile elements (Ti, Zr, Y, Hf, Th, Ta, Cr, Ni and REE) were used for discrimination of tectonomagmatic setting (Pearce and Cann, 1971; Pearce and Cann, 1973; Pearce and Norry, 1979; Wood, 1980; Pearce et al., 1981; Pearce, 1982; Shervais, 1982; Mullen, 1983; Pearce et al., 1984a; Meschede and Casey, 1986; Cabanis and Lecolle, 1989; Floyd et al., 1991).

Mantle Sequence

Serpentinized peridotite is characterized by low abundances of Si, Al, Ca, Na, K, and Ti and high abundance of in Mg, Cr and Ni.

Light rare-earth elements (LREE) concentrations are low, indication that serpentinization has not affected the original peridotite geochemistry. High degrees of serpentinization, especially where the fluid/rock ratio is large, mobilize LREEs in the serpentinizing fluid, resulting in U-shaped REE patterns that obscure the original igneous chemistry (Paulick et al., 2006). Li et al. (2006) show primary Al_2O_3 wt% is still preserved in peridotite with more than 90% serpentinization and no enrichment in LREE. Peridotites from the Eldivan ophiolite are extensively serpentinized but still show low LREE abundances and are therefore interpreted to have primary Al_2O_3 weight percents. This is important, as whole rock Al_2O_3 wt% is a proxy for degree of partial melting, as Al_2O_3 wt% decreases with high degrees of melt extraction, such as above a subduction zone (Bonatii and Michael, 1989). Eldivan ophiolitic mantle has Al_2O_3 wt% that range from 0.78-2.45, which is consistent with values from modern ocean floor and subduction-related mantle (Fisher and Engle, 1969; Ishii, 1985; Shibata and Thompson, 1986; Ishii et al. 1992; Seifert and Brunotte, 1996; Paulick et al., 2006) (Fig. 3).

Chromian spinel accessory minerals are also excellent indicators for degree of mantle extraction (Dick and Bullen, 1984). In Eldivan serpentinized peridotite, Cr#'s (Cr/Cr+Al) of Cr-spinel range from 0.47 to 0.70, which are in the range of type 2 and type 3 peridotite (Dick and Bullen, 1984). Cr#'s >0.6 (type 3) are categorized as arc peridotites and show the most depletion whereas type 2 are transitional between arc and MORB mantle. Eldivan mantle Cr-spinels overlap arc and MORB fields on Dick and Bullens's diagram for Cr-spinel Cr# v. Mg# (Fig. 4a). They also plot in the SSZ mantle field defined by Kamenetsky et al. (2001) on a TiO_2 wt% vs. Al_2O_3 diagram, with some points in the overlap between SSZ and MORB mantle fields (Fig. 4b).

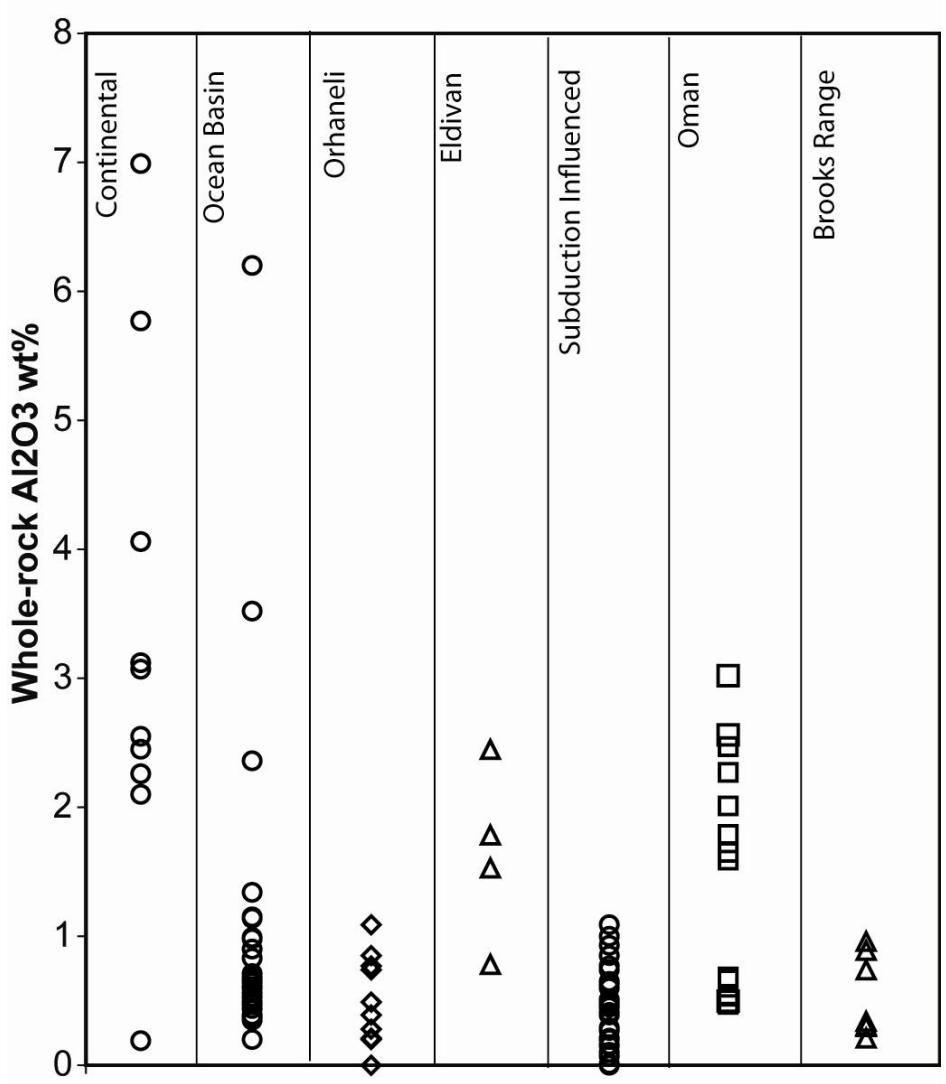

Figure 3. Whole rock Al_2O_3 wt% for mantle rocks from continental, ocean floor, and subduction trench settings compared to the Eldivan ophiolite mantle. Range in Al_2O_3 wt% in the Eldivan ophiolite spans the range of ocean floor and subduction trench mantle. It is also similar to that seen in the Oman ophiolite and somewhat higher than the Orhaneli ophiolite in the western İAESZ and the Brooks Range ophiolite in Alaska, interpreted to have formed in SSZ settings. Data sources for other mantle compositions are as follows: continental- Carter, 1970; Frey and Prinz, 1987; ocean floor- Shibata and Thompson, 1986; Paulick et al., 2006; Seifert and Brunotte, 1996; subduction trench- Fisher and Engle, 1969; Ishii, 1985; Ishii, 1992; Oman- Takazawa et al., 2003; Brooks Range- Harris, 1995; Orhaneli- Sarıfakıoğlu et al., in press.

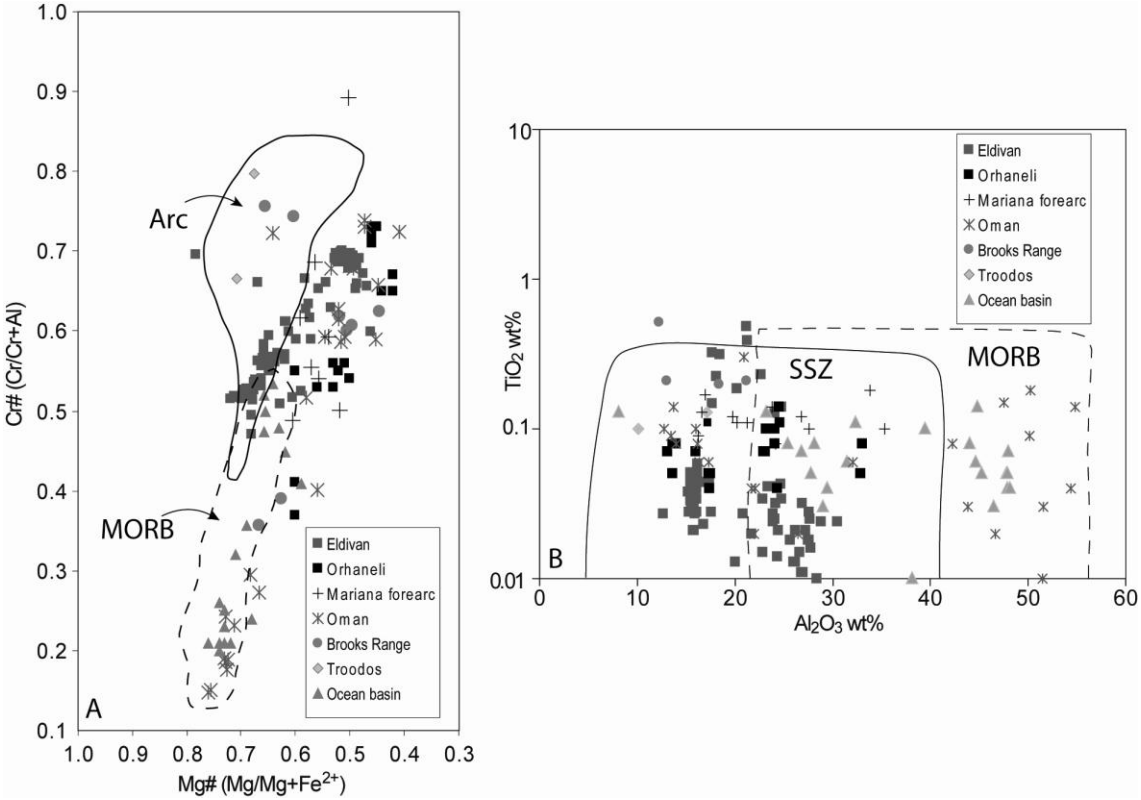

Figure 4. a) Cr#/ Mg# (Cr/Cr+Al and Mg/Mg+Fe^{2+}, respectively) of Cr-spinel the Eldivan serpentinized peridotite. Fields of abyssal (dashed line) and arc peridotites (sold line) are taken from Dick and Bullen (1984). b) TiO_2 wt% v. Al_2O_3 wt% in Cr-spinel of the Eldivan ophiolite. Fields of SSZ (solid line) and MORB (dashed line) are from Kamenetsky et al. (2001). Data is plotted with Cr-spinel data from the Orhaneli ophioilte (Sarıfakıoğlu, in press), Brooks Range ophiolite (Harris, 1995), ocean basin peridotites (Shiabata and Thompson, 1986; Morishita et al. 2007), Troodos, and Oman ophiolites (Augé and Johan, 1998; (Takzawa et al., 2003; Tamura and Arai, 2006) and Mariana peridotites (Ishii et al., 1992) for comparison. The Eldivan ophiolite plots mostly within the field of arc peridotites (a) and supra-subduction zone peridotites (b), indicating its subduction influenced character.

Crustal Sequence

Massive Gabbro

Most gabbro samples are 45 to 54 wt% SiO2 and are chemically classified as the plutonic equivalents of basalt and basaltic andesite (Fig. 5). A few samples have higher concentrations of alkalis, which could be a reflection of secondary albitization of plagioclase.

Gabbro has the lowest abundances of rare earth and trace elements of the crustal sequence, with elemental concentrations 1.5 to 5 times below N-MORB. REE patterns (Fig. 6a1) show lower LREE relative to heavy rare-earth elements (HREE), similar to N-MORB. Additionally, Th/Ta= 1.25-4.80, La/Nb= 0.54-1.91 and La/Yb=0.52-1.18 element ratios are generally low, similar to N-MORB. Sample 126a is the exception with higher LREE abundances relative to the HREE, perhaps from a subduction source, and high Th/Ta=9.10, La/Nb=3.00 and La/Yb=2.38 ratios. A few samples show flat REE patterns that could be a result of differentiation within the magma chamber.

Trace elements (Fig. 6a2) show scatter in mobile elements, particularly Rb, Ba, Th, U, K, and Sr, mostly likely due to secondary hydrothermal alteration. Most samples show the similar trace element pattern of large ion lithophile elements (LILE) depleted N-MORB, except sample 126a, which has a negative Nb anomaly again suggesting a subduction influence.

Dike rocks

Dikes are primarily basaltic andesite to andesite with a SiO2 range of ~ 56 to 58 wt% (Fig. 5). Element concentrations are most similar to N-MORB (2 times above and below N-MORB concentrations) compared to other units in the Eldivan ophiolite, with

REE patterns also similar to N-MORB (Fig 6b1). Low ratios of Th/Ta= 0.82-4.40, La/Nb= 1.22-1.93 and La/Yb are similar to massive gabbro values and again

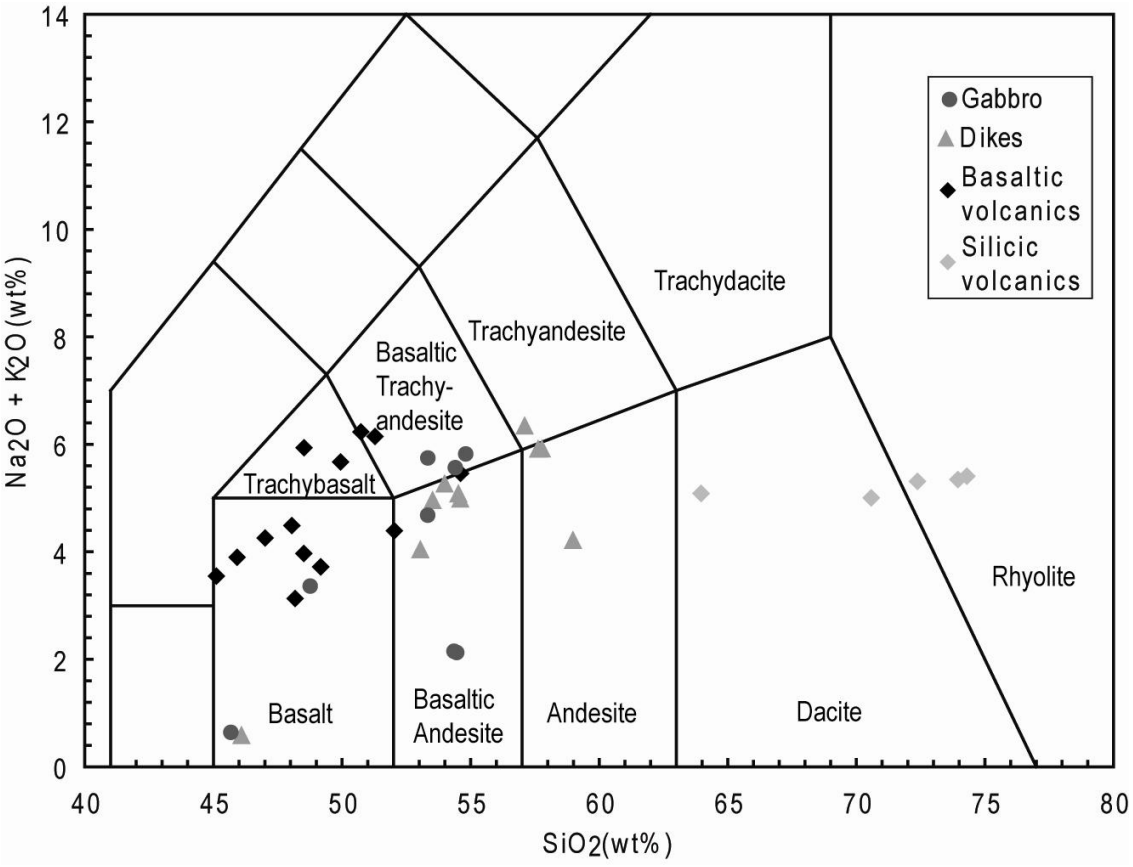

Figure 5. IUGS Total alkali silica classification diagram illustrating the distribution of rock types in the Eldivan ophiolite. Volcanic rocks are basaltic and rhyolitic, while dike rocks plot between the two in the basaltic andesite and andesite fields.

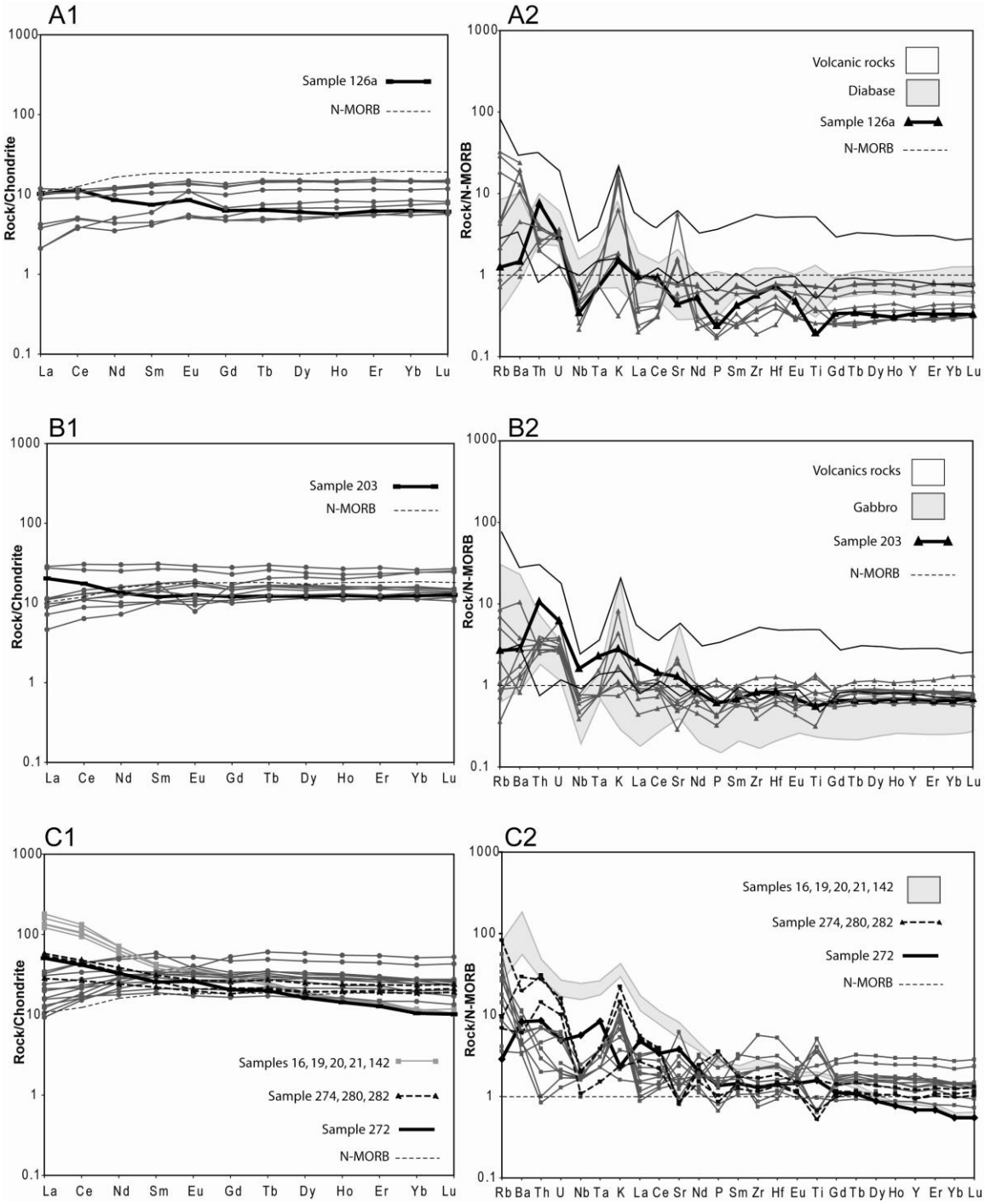

Figure 6. REE (1) and incompatible element diagrams (2) for a) gabbro, b) dikes, and c) volcanic rocks. REE elements were normalized to chondritic meteorite compositions (McDonough and Sun, 1995). N-MORB reference line (Sun and McDonough, 1989) is marked by a thin dotted line on all diagrams.

near N-MORB. One exception is sample 203, which shows a slight elevation in LREE, with no depletion in the HFSE, similar to E-MORB (Sun and McDonough, 1989). Th/Ta and La/Nb ratios in this sample are similar to the other dikes, although La/Yb= 2.42 is higher, reflecting the higher LREE concentrations.

Trace element patterns (Fig. 6b2) show characteristic N-MORB low LILE abundances compared to the HREE, with hydrothermal alteration reflected in varying concentrations of mobile Rb, Ba, Th, U, K, and Sr. As seen in the REE, sample 203, shows higher concentrations of LILE beginning with Nb and sloping downward to the HREE with a slight increase in Hf and Zr. The absence of a negative Nb-Ta anomaly suggests that higher values of LILE are not due to a subduction component, but perhaps a less depleted mantle source.

On tectonic discriminant diagrams, dike rocks plot in fields of supra-subduction zone (SSZ) (Fig. 7 A, F), island-arc tholeiites (IAT), (Fig. 7 B, C, G) and back-are basin basalt (BABB) (Fig. 7 D, E), and show some overlap into areas where subduction-influenced and MORB fields overlap (Fig. 7 B, D, G). Dikes plot consistently in the SSZ and back-arc basin field in diagrams E and F (Fig. 7), which use the most immobile trace elements of La, Nb, and Yb to infer tectonomagmatic setting. Additional ternary discriminant diagrams (Fig. 8) also plot dikes in subduction related fields. On diagrams B and C, dikes plot almost entirely as island arc basalt and island arc tholeiites, respectively. Diagram D has scatter between the BABB and MORB fields, while A and E do not discriminate between subduction and MORB basaltic rocks.

Volcanic Rocks

Major element chemistry reveals a bi-modal distribution of volcanic rocks: basalt to trachybasalt and dacite to rhyolite. Basaltic rocks contain 45-53 wt% SiO2 and plot mainly in the basalt field on the total-alkali silica diagram with some overlap in to the basaltic andesite field (Fig. 5). Rhyolitic rocks contain 63 to 74 wt% SiO2 and fall into rhyolite and dacite fields (Fig. 5). Basalts show three distinct geochemical signatures:

(1) The most dominant pattern, seen in samples 2, 3, 4, 5a, 5b, 10, 11, 88 and 220, shows LREE depletion characteristic of N-MORB (Fig. 6c1), with low ratios of Th/La = 0.33-2.05, La/Nb= 0.56-2.10 and La/Yb= 0.49-1.29. Element concentrations are equal to and up to 3.5 times more than N-MORB concentrations, giving these basaltic rocks the highest elemental concentrations when compared to the massive gabbros and sheeted dikes.

The trace element diagrams for these basaltic volcanics (Fig. 6c2) show a large amount of variation, particularly with mobile elements of Rb, Ba, Th, U, K and Sr, which reflect their alteration. However, patterns still show the low LILE abundance (compared to HREE) that is typical of N-MORB.

Discriminant diagrams for N-MORB-like basaltic rocks show more scatter than dike rocks, but plot in fields of MORB more often than subduction-influenced fields (Fig. 7 A-G). In diagrams C, E, and B, basaltic rocks plot almost entirely within the MORB field, while some samples plot close but somewhat outside MORB fields in B, D, and G. On diagrams E and F which use the most immobile elements, most basalt samples plot in the MORB field. Ternary discriminant diagrams have similar results (Fig. 8) with basalts

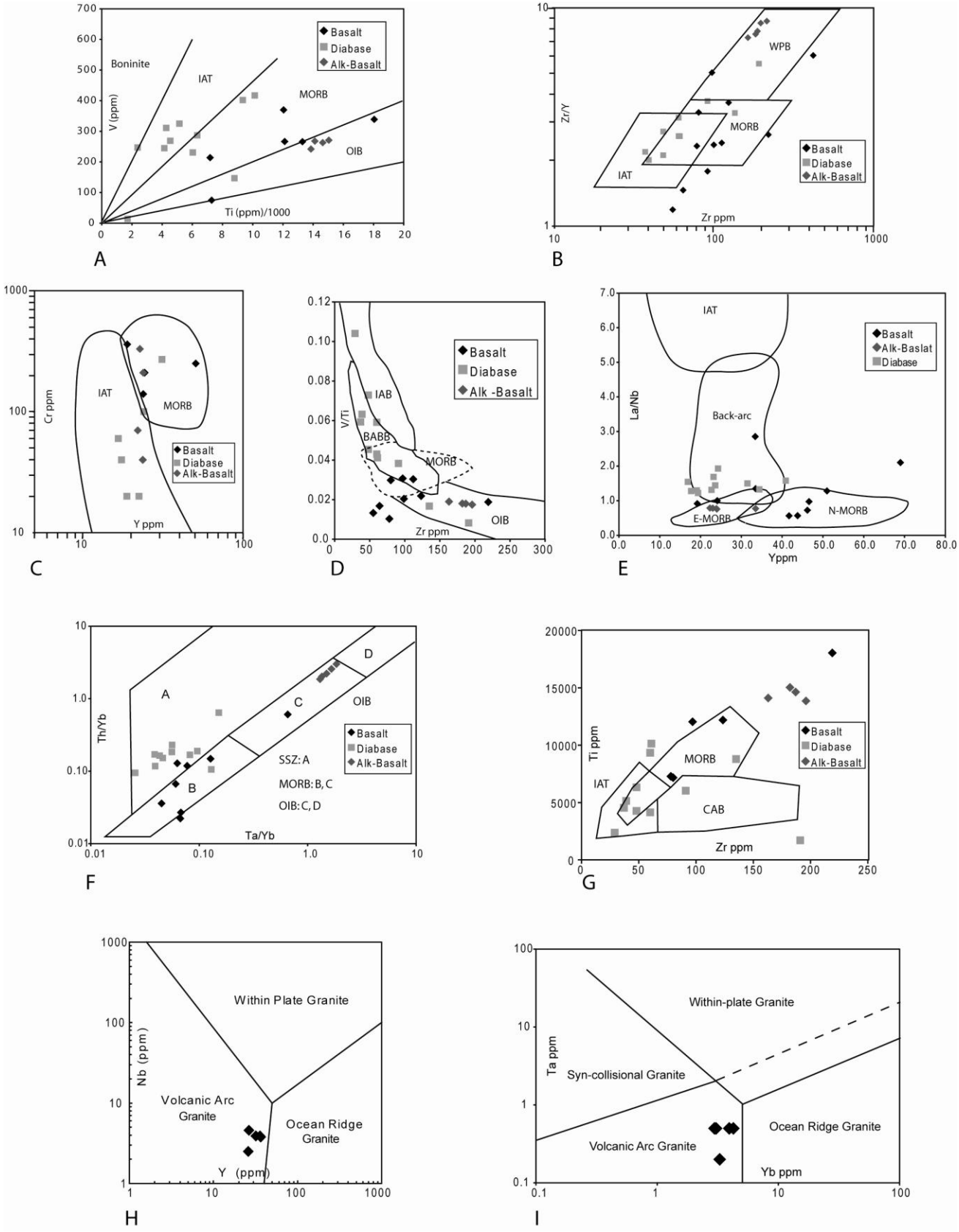
A
Boninite
IAT
MORB
OIB
V (ppm)
Ti (ppm)/1000
Basalt
Diabase
Alk-Basalt
B
WPB
MORB
IAT
Zr/Y
Zr ppm
C
IAT
MORB
Cr ppm
Y ppm
D
IAB
BABB
MORB
OIB
V/Ti
Zr ppm
E
IAT
Back-arc
E-MORB
N-MORB
La/Nb
Yppm
Alk-Baslat
F
A
B
C
D
OIB
SSZ: A
MORB: B, C
OIB: C, D
Th/Yb
Ta/Yb
G
IAT
MORB
CAB
Ti ppm
Zr ppm
H
Within Plate Granite
Volcanic Arc Granite
Ocean Ridge Granite
Nb (ppm)
Y (ppm)
I
Within-plate Granite
Syn-collisional Granite
Volcanic Arc Granite
Ocean Ridge Granite
Ta ppm
Yb ppm

Figure 7. Nine discriminate diagrams for basaltic rocks of the Eldivan ophiolite. In diagrams a-g, basaltic rocks generally plot in MORB fields, although some show too much scatter to be conclusive. Dikes mostly fall into island arc tholeiite (IAT) fields with some over lap in MORB fields. Alkaline basalts plot consistently in ocean island basalt (OIB) or with-in plate basalt (WPB) fields. Diagrams h and i are for granitic rocks. Samples from the Eldivan ophiolite all plot in volcanic arc granite fields. These diagrams are from a) Shervais, 1982; b) Pearce and Norry, 1979; c) Pearce, 1982; d) Woodhead et al., 1993 and Floyd et al., 2000; e) Floyd et al., 1991; f) Pearce et al., 1981; g) Pearce and Cann, 1973; h) Pearce et al., 1984a; i) Pearce et al., 1984a. Abbreviations: Island arc tholeiite (IAT), ocean island basalt (OIB), with-in plate basalt (WPB), back-arc basin basalt (BABB), enriched MORB (EMORB), normal MORB (N-MORB) supra-subduction zone (SSZ) and continental arc basalt (CAB).

falling clearly into the MORB fields on diagrams B, C, D. Diagrams A and E do not distinguish between MORB and subduction related basaltic rocks.

(2) Contrastingly, the geochemistry of samples 16, 19, 20, 21 and 142 shows very elevated immobile LREE up to 17 times that of N-MORB and REE below N-MORB concentrations, giving steeply sloping patterns typical of alkaline ocean island basalts (OIB) (Fig. 6c). Element ratios of La/Yb are correspondingly high (La/Yb= 16.21-22.47). Sample 272 shows low abundances in HREE but only a moderate LREE elevation, comparable to transitional arc basalts (Fig. 6c) (Pearce et al., 1982).

Trace element patterns for these alkaline rocks show the same elevation in the LILE as see in the LREE, with some variation in mobile elements. Sample 272 has LILE abundances more elevated than the N-MORB-type basalts, but less than the alkaline rocks. Absence of a Nb anomaly combined with the low HREE concentrations suggests this samples source was not modified by a subduction component but perhaps by a source more enriched than an N-MORB source.

These rocks consistently plot in fields for OIB, within plate basalt, and alkaline basalt on discriminant diagrams (Fig. 7 A, B, D, F). In diagrams where alkaline fields are not present, these rocks plot outside all fields (G) or overlap both the IAT and MORB

fields (C), and cannot be discriminated. In diagram E, these samples plot in the E-MORB field. Similar results are seen with additional ternary discriminant diagrams (Fig. 8).

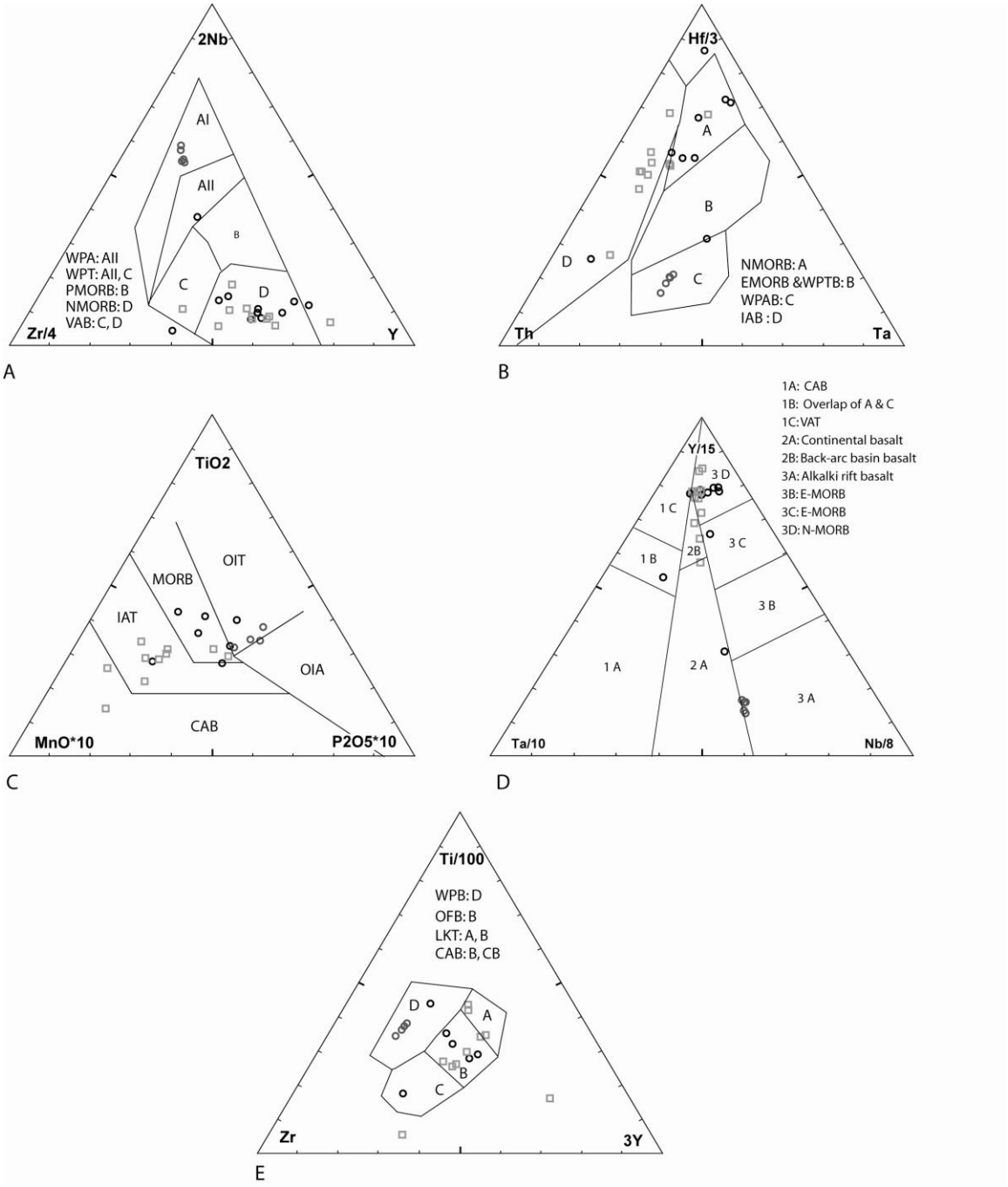

Figure 8. Discriminant ternary diagrams for basaltic rocks of the Eldivan ophiolite. Basaltic rocks are open black circles, dikes are gray squares, and alkaline basalt are gray circles. In diagrams a-e, basaltic rocks fall mostly into the field of MORB with little overlap into subduction influenced fields. On diagrams that do not distinguish between MORB and subduction fields, basalts plot in both fields. Dikes from the Eldivan ophiolite fall into subduction related fields on diagrams that distinguish between MORB and arc related rocks. On those that do not, dikes plot in the MORB-arc fields. Alkaline basalts consistently plot in

enriched ocean island or with-in plate basalt fields. Abbreviations: With-in plate alkaline basalt (WPA), with-in plate tholeiitic basalt (WPT), with-in plate basalt (WPB), ocean island tholeiite (OIT), ocean island alkalic basalt (OIA), plume-MORB (PMORB), volcanic arc basalt (VAB), enriched MORB (EMORB), island arc basalt (IAB), continental arc basalt (CAB), volcanic arc tholeiite (VAT), ocean floor basalt (OFB), and low-K tholeiite (LKT). Fields are from a) Meschede and Casey, 1986; b) Wood, 1980; c) Mullen, 1983; d) Cabanis and Lecolle, 1989; e) Pearce and Cann, 1971.

In all diagrams, these rock plot as within plate alkali (A, B, D), ocean island tholeiite (C), and within plate basalts (E).

(3) The third geochemical signature is seen in basaltic sample 274, which shows LILE enrichment and HFSE (Nb, Ta) depletion relative to N-MORB, suggesting a subduction- influenced source (Fig. 6c2). A subduction-influenced source is also reflected in a slight LREE enrichment and high ratios of Th/La (6.48), La/Nb (2.85) and La/Yb (3.66) (Fig. 6c1).

Rhyolitic samples 280, 282, 293, 293c and 293d have two separate trace and REE signatures. Samples 280 and 282 closely match basaltic sample 274. LREE abundances are elevated, reflected in Th/Ta, La/Nb, and La/Yb ratios similar to sample 274 (Fig. 6c1). LILE (Fig. 6c2) are also more abundant except for negative concentrations of Nb, Ta, and Ti, characteristic of subduction zones. Some scatter is still seen in the mobile elements, particularly Rb, K, and Sr.

Samples 293, 293c, and 293d are similar to N-MORB in their lower LREE concentrations compared to HREE (Fig. 6c1), but have overall flatter patterns that could reflect higher degrees of differentiation in the magma chamber. This same pattern is also seen in the trace elements (Fig. 6c2), with LILE slightly lower in concentration than the HREE, with the exception of Zr and Hf that show higher abundances. The effects of secondary alteration are seen in scatter of mobile elements, especially Ba, U, Th, K, and Sr.

Despite the two signatures seen in REE and trace elements, all of the rhyolitic samples plot in fields for volcanic arc granite (Fig. 7, H, I) on discriminant diagrams of Pearce et al. (1984a) that are based on immobile elements of Nb, Ta, and Yb.

INTERPRETATION OF WHOLE-ROCK AND MINERAL CHEMISTRY

Three different magma affinities are present in the Eldivan ophiolite: N-MORB, alkaline (OIB), and SSZ. The occurrence of three distinct geochemical signatures in this small area of exposure (~20 km^2) implies a high degree of mixing of either: 1) upper and lower plate blocks during tectonic emplacement or 2) magma sources during seafloor formation.

Mixing of upper and lower plate units is plausible, considering the current imbricated structure of the ophiolite in the mélange. This has been suggested to account for alkaline rocks within the mélange that are interpreted as seamounts accreted into the serpentine mélange from the down-going plate (Floyd, 1993; Tüysüz et al., 1995; Tankut et al., 1998). Accretionary mixing of an N-MORB down-going plate, which included seamounts, with a SSZ upper plate could explain the geochemical variation in the Eldivan ophiolite, although few modern analogs of this process exist.

Similar chemical variations to those seen in the Eldivan ophiolite are found in modern back-arc SSZ basins due to mixing different magma sources rather than upper and lower plate components. SSZ or back-arc ocean basins are extensional upper plate basins that form above subduction zones due to lower plate movement away from the upper plate through slab roll-back. The combination of extension and subduction in SSZ back-arc settings creates conditions of both mantle depletion and enrichment that result in basalts of different compositions (Sinton and Fryer, 1987; Price et al., 1990; Stern et al.,

1990; Eissen et al., 1994; Hawkins and Melchior, 1985; Dril et al., 1997; Fretzdorff et al., 2002; Sinton et al., 2003). Basalt in the North Fiji, Lau, Mariana, Manus, and East Scotia back-arc basins show and overprint of LILE enrichment on N-MORB geochemical patterns, which increase with proximity to the subducting slab. Compositional zoning in the Lau basin, with LILE enriched basalt on the west edge near the arc and N-MORB types in the young central spreading center, show that LILE enrichment decreases as rifting continues due to decreased subduction influence from slab roll back (Hawkins and Melchior, 1985; Pearce et al., 1984b). Likewise, initial rifts in the Mariana Trough erupt basalt similar to the Mariana arc, where older rift zones erupt N-MORB (Stern et al., 1990). North Fiji and East Scotia spreading ridges erupt basalt transitional between N-MORB and alkaline basalt due to influence from hot spot volcanism (Price et al., 1990; Eissen et al., 1994; Freztdorff et al., 2002). This chemical array is similar to that seen in the Eldivan ophiolite and occurs entirely in the upper plate, due to mixing of variably depleted and enriched mantle sources or melts (Sinton and Fryer, 1987; Price et al., 1990; Stern et al., 1990; Dril et al., 1997).

In this study, the back-arc basin or SSZ mixing is favored for the Eldivan ophiolite. While incompatible and REE diagrams are dominated by N-MORB patterns, there are noticeable subduction and alkaline influences (samples 126a, 203, 280 and 272), as seen in modern back-arc and intra-arc settings. Additionally, basalt mostly plots as N-MORB, with some scatter into other fields (Fig. 7 and Fig 8) but dike rocks plot consistently within subduction influenced fields, including island arc tholeiite (IAT), back-arc basin, and SSZ, with minor overlap into N-MORB fields (Fig. 7and Fig 8). These dike compositions patterns provide direct evidence that the Eldivan ophiolite was

at one time in a supra-subduction setting, as the sheeted dike complex represents ocean floor construction. Additionally, rhyolitic volcanics also plot in volcanic arc fields (Fig. 7), giving more evidence for a significant subduction influence.

Evidence for a supra-subduction zone setting is also found in the mantle sequence of the Eldivan ophiolite. Cr-spinel (Cr#'s 0.47 to 0.70) plot within fields for mantle more depleted than ocean rift mantle, closer to transitional supra-subduction settings (Fig. 4) similar to Oman-type ophiolites as defined by Harris (1992). This is also supported in whole rock Al_2O_3 wt% of the Eldivan ophiolite, which indicates the degree of partial melt extraction, and could be expected for ocean crust in the complex melting regime of a back-arc basin. It also closely matches Al_2O_3 wt% concentrations from the Oman ophiolite but is slightly higher than the Brooks Range ophiolite and Orhaneli ophiolite (western İAESZ), all thought to have formed in a supra-subduction zone settings (Fig. 3).

Finally, a SSZ interpretation is consistent with other studies along the İAESZ in the Ankara mélange, Dağkuplu mélange and Kırşehir block ophiolitic massifs. Other areas of the Ankara mélange contain alkaline basalts (Çapan and Floyd, 1985; Floyd, 1993; Tankut et al., 1998), N-MORBs (Tankut, 1984; Tankut et al., 1998), and IAT basalts (Tankut, 1984; Tankut et al., 1998; Tüysüz et al., 1995) similar to the Eldivan ophiolite. Our discovery of SSZ dikes is consistent with the discovery of SSZ plagiogranite in the Ankara mélange (Dilek and Thy, 2006). Similarly, the Dağkuplu mélange in the western İAESZ show the same variety of alkaline, N-MORB, and SSZ geochemistry (Göncüoğlu et al., 2006; Sarıfakıoğlu, 2006; Sarıfakıoğlu et al., in press). Supra-subduction geochemistry also characterizes Cretaceous ophiolites from the

Kırşehir block (Çiçekdağ and Sarıkarıman massifs) (Yalınız et al., 1996; Floyd et al., 2000; Yalınız et al., 2000a).

Most of these previous studies use geochemistry of crustal volcanic rocks, cumulate sequences, dike complexes, and massive gabbros for their interpretation without data from associated mantle peridotite. Including analyses of the peridotite provides additional evidence for high degrees of melt extraction inconsistent with a MORB tectonic model for the Eldivan ophiolite. Sarıfakıoğlu et al. (in press) used both mineral and whole-rock geochemistry of crust and mantle rocks to interpret the Orhaneli ophiolite in the western İAESZ as a supra-subduction zone ophiolite. Cr-spinel data from lherzolite and harzburgite of the Orhaneli mantle sequence closely match the Eldivan ophiolite (Fig. 4). Whole-rock Al_2O_3 from the Orhaneli ophiolite is generally lower, but still with in the range of the Eldivan ophiolite (Fig. 3). These results show the same continuity in mantle composition as seen in the crustal sequence geochemistry data that argue for some supra-subduction influence from the western to central İAEO.

AGE AND SOURCE TERRAINS OF EPI-OPHIOLITIC COVER

Sandstone samples were collected from a block within the Ankara mélange immediately adjacent to basalt and from the Karadağ Formation which unconformably overlies the mélange. Age and tectoinc source region for sandstone samples from the mélange and overlying Karadağ Formation were investigated through detrital zircon and sandstone petrography. Siliciclastic material was very scarce and these two samples represent the only sandstones found within the study area. The entire sample collected was processed for detrital zircons. The error introduced by the limited sample size and small number of zircons found with in each sample is recognized, however the results

obtained are consistent with age data obtained through other methods throughout the suture zone.

Zircon U-Pb age analyses were conducted by laser ablation multicollector inductively coupled plasma mass spectrometry (LA-MC-ICPMS) at the Arizona LaserChron Center. Analytical methods follow those described in Gehrels (2000) and Gehrels et al. (2006). Single point analyses were taken with a 35 and 25 micron diameter beam according to grain size. Common Pb corrections are for ^{204}Pb, using an initial Pb composition from Stacey and Kramers (1975). Uncertainties are 1.0 for ^{206}Pb/ ^{204}Pb, 0.3 for ^{207}Pb/ ^{204}Pb, and 2.0 for ^{208}Pb/ ^{204}Pb. Detrital zircon age extractor and ISOPLOT 3.00 (Ludwig, 2003) were used to determine and sort reliable age data. Detrital zircon age extractor extracts significant peak ages based on at least three grain analyses and the number of grains constituting each peak age. Results are listed in Table A3.

Detrital Zircons

Detrital zircon age populations from sandstone in the mélange and Karadağ Formation have different minimum, maximum, and peak ages, suggesting they were sourced from different terrains (Fig. 9). Detailed analysis of the mélange sandstone shows and age distribution from 143.2 (±2) Ma to 164.1 (± 1) Ma with a peak age of 153 Ma. The Karadağ sandstone shows an age distribution from 105.2 (±5) Ma to 166 (±3) Ma with a peak age of 130 Ma. The youngest peak age is used here as a proxy for the maximum age of deposition, which is consistent with the stratigraphic positions of the sandstones. The maximum age of the mélange sandstone, and Eldivan ophiolite, is 143.2 (±2) Ma, while the maximum age of the Karadağ sandstone is 105.2 (±5) Ma. Peak ages

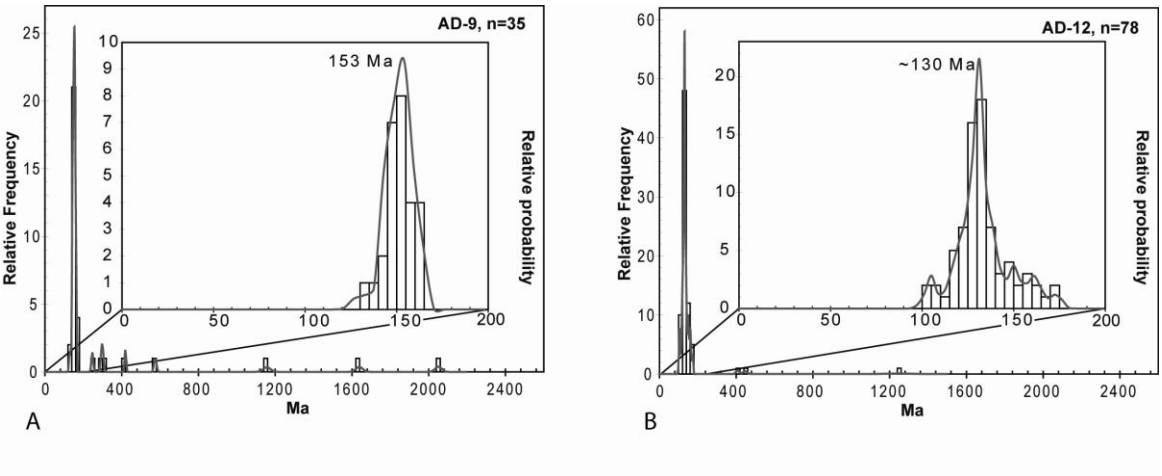

Figure 9. Detrital zircon age populations for sandstones within the mélange (a) and the Karadağ Formation (b) indicating different source terrains for the two units. The larger graphs show the entire zircon population including those that have Precambrian ages. The inset graph shows the detail of the peak ages. For the ophiolitic sandstone, the distribution of ages is narrow with a peak age of ~153 Ma. The Karadağ sandstone has a larger range in ages and a peak age of ~130 Ma.

here are interpreted to represent the average age of the terrain dominantly being eroded at the time of deposition.

An inherited fraction of zircon from Neo to Paleo- Proterozoic is present in both mélange and Karadağ sandstones (Fig. 9). Detrital zircons of similar age from the Tauride block in southwestern Turkey are documented by Kröner and Şengor (1990), who attribute them to the southern Angara craton of Siberia. Dilek and Thy (2006) also found Proterozoic zircon in plagiogranite from the ophiolite near Ankara and interpret them as a subduction recycled component from the Rhodope-Strandja Massif in northwest Turkey and southeast Bulgaria. These terrains may also have supplied the Paleo- to NeoProterozoic zircon grains in the mélange and Karadağ sandstones.

Sandstone Petrography

Sandstone from both formations are compositionally and texturally immature with low percentages of quartz and angular to sub-angular clasts. Despite alteration and secondary authigenic growth, the sandstone samples yield two very different petrographic

provenance results. The mélange sandstone is dominated by volcanic lithic fragments (52.33 %) and plagioclase (25.33%), with minor quartz (8.66%), K-feldspar (2.00%), and some clay minerals (11.66%). In contrast, the overlying Karadağ sandstone is made up of carbonate mud clasts (with some authigenic clay) (45.33%), plagioclase (28.00%), bioclastic grains (15.00%), and quartz (11.33%), with minor volcanic lithic material (0.33%).

Composition of the mélange sandstone implies it was sourced from a nearby volcanic terrain, according to tectonic discriminant diagrams of Dickinson et al. (1983) (not shown). There are a number of sources for lithic fragments in the İzmir-Ankara-Erzincan ocean including seamounts, island arcs (Tankut, 1984; Tankut et al., 1998; Tüysüz et al., 1995), and the Pontide continental arc to the north. However, the Pontide arc is younger (Turonian) than detrital zircon grains found in the mélange sandstone, suggesting it is not the source for volcanic lithics. The other plausible volcanic sources are oceanic, giving more evidence for and intra-oceanic subduction away from the continental margin. Sandstone from the Karadağ Formation contains virtually no volcanic lithics, bioclastic grains, carbonate mud, and plagioclase grains. The bioclastic material in this sample is a mix of echinoderm, bryozoan, brachiopod, bivalve, and foraminifera grains, a compositional variation that suggests a well developed but relatively shallow carbonate system. No deep water fauna are present. This data suggests that the Karadağ sandstone was derived from the carbonate system of a continental margin and was deposited in a nearby marginal basin. This is consistent with the interpretation of the Karadağ Formation as flycsh deposited on the imbricated

ophiolite, most likely in a fore-deep setting near the continental margin created as continuing subduction brought the Kırşehir and Sakarya-Pontide terrains together.

STRUCTURE OF THE ELDIVAN OPHIOLITE

The angular conformable relationship of the Karadağ Formation with the underlying imbricated mélange and subsequent imbrication of the mélange with the Karadağ Formation imply at least two phases of deformation (Fig 10). The first phase imbricated and rotated the ophiolite which thrust serpentinite between its units (Fig 10a). Thrust faults in the imbricated ophiolitic mélange have been rotated to vertical, as have pillow basalts and sheet flows that constrain paleohorizontal. Structure like this can be created in the hinterland of an accretionary wedge, where underthrusting of the wedge front back-tilted the hinterland, rotating the ophiolite from its original position. Rotation of the sheeted dike complex, discussed below, also occurred during this deformation phase. This deformation would result in sub-horizontal fold hingelines, however, no fold hingelines are present in this area. Field work in additional areas in the Ankara Mélange is needed to resolve this issue.

The second phase of deformation occurred after the Karadağ Formation was deposited on top of the imbricated ophiolite and thrust the Karadağ Formation with the underlying ophiolite and serpentine along southward verging thrust faults (Fig 10b). Some age constraints for these events are provided by detrital zircon populations from the mélange and Karadağ sandstones. Restoration of these deformation events is possible through controls of pillow basalts, sheet flows, and the sheeted dike complex.

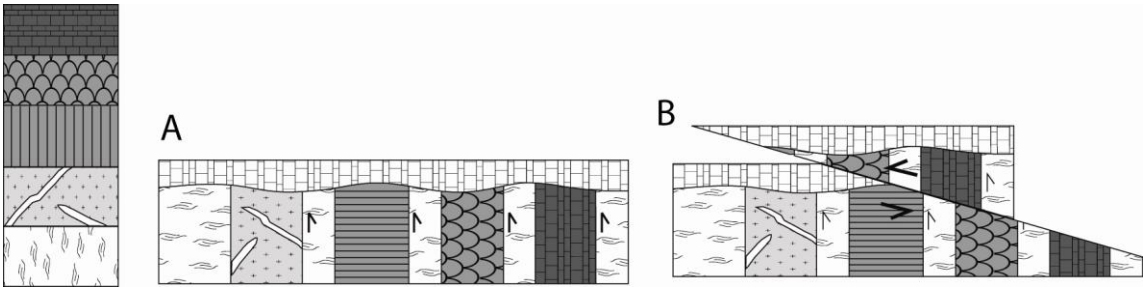

Figure 10. Two deformation phases took place in the Ankara Mélange. The first imbricated and rotated the ocean crust from its original structure to a position like shown in the first deformation phase (a). The second phase of deformation thrust the unconformable Karadağ Formation in with the underlying imbricated ophiolite (b).

Timing of ophiolite imbrication

Initial imbrication of the Eldivan ophiolite must have occurred between 143 (±2) Ma, the age of the melange sandstone, and 105 (±5) Ma, the age of the overlying Karadağ sandstone. Further imbrication of the ophiolite and the Karadağ Formation occurred sometime after 105 (±5) Ma. Imbrication of the Eldivan ophiolite between 143 (±2) and 105 (±5) Ma is consistent with data from other parts of the suture zone that suggest collapse of the ocean basin had begun around this time. For example, radiolaria in limestone deposits from the Kirazbaşı foredeep complex are as old as ~135 Ma (Late Valanginian) (Tüysüz and Tekin, 2007). Intra-oceanic thrusting began prior to 90 Ma near the Kırşehir block (Yalınız et al., 2000b) and 93 (±2) Ma in the western İAEO (Önen, 2003). Granitoids 94.9 (±3.4) Ma of the Kırşehir block interpreted as the result SSZ ophiolite obduction also suggest subduction must have been active before 95 Ma (Boztuğ et al., 2007).

Restoration of the Eldivan ophiolite

The orientation of sheeted dikes in ocean crust is commonly used as a proxy for spreading ridge orientation. For the Eldivan ophiolite, it would represent the orientation

of a back-arc or intra-arc spreading ridge. The ideal structural relationship of sheeted dikes to the overlying basalts they feed is perpendicular. Dikes in the ophiolite have two different orientations, roughly NNW-SSE and E-W and are dipping steeply (Fig. 11a and Table 1), except in one locality where they NNW-SSE and near horizontal. The near horizontal feeder dikes are perpendicular to pillow basalts and sheet flows that have been rotated to vertical, indicating that the dikes have rotated 90° about a horizontal axis. Paleomagnetic data indicate that the Ankara Mélange near the Eldivan ophiolite has undergone an additional rotation about a vertical axis due indentation of the Kırşehir block during its collision with the Sakarya-Pontide terrain (Kaymakci et al., 2003). Using pillow basalts and limestone beds as paleo-horizontal indicators in conjunction with the paleomagnetic data, the sheeted dike complex can be restored to its original position and infer the orientation of back-arc spreading for the Eldivan ophiolite.

When rotated 90° about a horizontal axis, horizontal E-W and steeply dipping N-S dikes restore as vertical and near vertical dikes with an average strike of 188 degrees (Fig. 11b) whereas the E-W vertical dikes restore to near horizontal, most likely sills or sheet flows, and are therefore not indicative of a spreading orientation. An additional rotation of the dikes is needed to restore the dikes to their position prior to indentation of the Kırşehir block. According to Kaymakci et al., (2003) the Çankırı basin experienced rotation during the Eocene Epoch through the mid- Miocene and perhaps as early as the Paleocene Epochs. Near the Eldivan ophiolite, the Çankırı basin margin rotated 33° counterclockwise during Oligocene time. Restoration of the Eldivan ophiolite spreading ridge as a result of this rotation reveals a spreading ridge orientation of 222 degrees, or NE-SW (Fig 11c). This indicates that intra-oceanic subduction of the Eldivan ophiolite

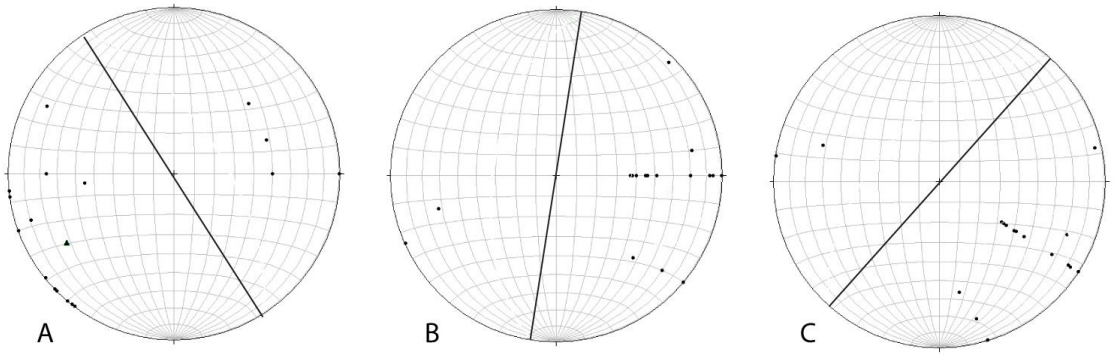

Figure 11. Orientation of spreading ridge in the Eldivan ophiolite a) prior to any restoration, b) restored about a horizontal axis according to paleo-horizontal controls and **c)** restored to its original orientation by further rotation about a vertical axis, controlled by paleomagnetic data. Solid black lines on each stereograph represent the average strike of the spreading ridge.

Table 1. Structural measurements

Strike	Dip		Strike	Dip		Strike	Dip		Strike	Dip		Strike	Dip		Strike	Dip	
120	80	S	270	70	NE	353	78	E	277	54	N	342	80	E	310	90	
120	75	S	275	45	S	28	76	E	280	65	N	40	50	E	317	52	SW
123	50	S	160	50	S	193	90		276	50	N	308	90		0	90	
104	70	S	162	42	S	160	90		280	68	N	340	90		0	90	
11	90		174	45	NE	140	80	NE	275	90		352	90		0	50	NE
65	90		182	40	NE	321	90		276	63	S	1	90		316	90	
128	90		174	90		307	90		282	67	S	180	66	E	320	90	
118	90		15	90		315	90										

SSZ basin was oblique to the Sakarya-Pontide terrain, creating a back-arc spreading ridge at an angle to the continental margin. However, paleodeclination data of Kaymakci et al., (2003) indicate rotation may have taken place as early as Paleocene time or before. This would mean additional clockwise rotation is needed to restore the true orientation of the spreading ridge. The Ankara Mélange appears to be rotated nearly 90° from the overall E-W orientation of the suture zone, which could indicate an additional 60° rotation of the Eldivan ophiolite is needed. This would mean the spreading ridge and intra-ocean subduction zone were orthogonal to the Sakarya-Pontide continental margin, indicating little strike slip motion in the creation of the suture zone. This is consistent with Fayon et

al., (2001) and Whitney et al. (2001) who found the northern portion of the Kırşehir block was deformed and exhumed by orogen-normal collision.

TECTONIC EVOLUTION

Review of the İAEO

Understanding the overall tectonic evolution of the İAEO is crucial to reconstructing the role played by the Eldivan ophiolite. Age constraints of various events throughout the İAESZ indicate three main phases of İAEO evolution: a constructional phase, destructional phase, and suturing phase (Fig. 12a).

The constructional phase began with rifting at least as old as Late Carnian-Early Norian stages (~215 Ma), based on radiolaria associated with MORB in the central and western part of the suture zone (Bragin and Tekin, 1996; Tekin et al., 2002). Other radiolaria suggest it developed into an ocean basin by Late Bajocian time (Tüysüz and Tekin, 2007) and seamounts formed on the ocean floor during the Jurassic and Cretaceous Periods (Rojay et al., 2001; Rojay et al., 2004; Tankut et al., 1998).

Destruction of the ocean basin by intra-oceanic subduction is documented by SSZ ophiolites, the oldest located in the Ankara Mélange yielding a U/Pb zircon age of 179 (±15) Ma (Dilek and Thy, 2006). Intra-oceanic subduction continued through the late Cretaceous Period, creating SSZ ocean crust in the central İAEO, now part of the Kırşehir block (Yalınız et al., 1996; Yalınız et al., 2000b), and the Dağkuplu mélange (Göncüoğlu et al., 2006; Sarıfakıoğlu, 2006; Sarıfakıoğlu et al., in press). Late Valanginian (~135 Ma) (Tüysüz and Tekin, 2007) to Paleocene ge (Koycigit, 1991) radiolaria are found in foredeep deposits along the Sakarya-Pontide margin suggest active subduction against the continent began in the early Cretaceous Period. Other events documenting subduction at

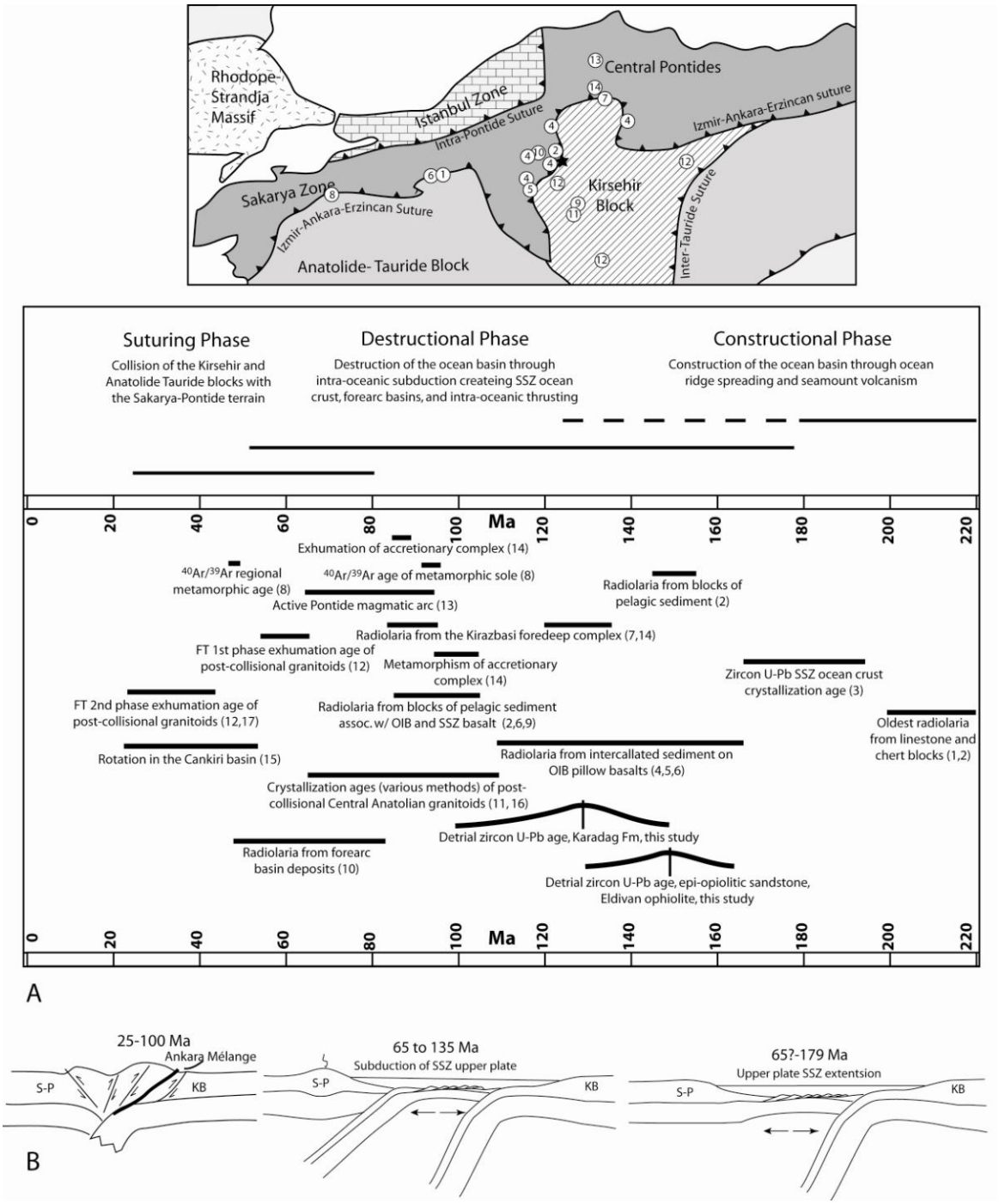

Figure 12. a) Age constraints for the evolution of the İAESZ through time. Three main phases are identified: 1) an initial construction phase where the ocean basin was forming through ridge spreading with hotspot volcanism creating seamounts on the ocean floor; 2) destruction of the ocean basin through intra-oceanic subduction that resulted in intra-oceanic sea floor spreading above a subduction zone and arc magmatism 3) collision and suturing of the Kırşehir and Anatolide-Tauride continental blocks with the Sakarya-Pontide terrains. Numbers on the timeline and map correspond to the source of age data (below) and sample locations, respectively. The sample location for detrital zircons of this study is represented with a black star. Sources for data are as follows: 1) Tekin et al., 2002; 2) Bragin and Tekin, 1996; 3) Dilek and Thy, 2006; 4) Rojay et al., 2004; 5) Rojay et al., 2001; 6) Göncüoğlu et al., 2006; 7) Tüysüz and

Tekin, 2007; 8) Önen, 2003; 9) Yalınız et al., 2000; 10) Koçyiğit, 1991; 11) Yalınız et al., 1999; 12) Boztuğ and Jonckheere, 2007; 13) Yılmaz et al., 1997; 14) Okay et al., 2006; 15) Kaymakci et al., 2003; 16) Boztuğ et al., 2007 and references therein; 17) Fayon et al., 2001. b) Schematic cartoon model for the evolution of the Eldivan ophiolite during the Cretaceous using the Philippine Sea plate and Mariana trough as an analogue. Early Cretaceous time documents the beginning of subduction and upper plate extension as evidenced by SSZ basalt, foredeep complexes along the continental margin, and ophiolitic metamorphic soles. Late Cretaceous is the beginning of SSZ upper plate subduction along the Sakarya-Pontide margin, causing active volcanism in the Pontide continental arc. Latest Cretaceous through Oligo-Miocene is characterized by collision and suturing of the Kırşehir block and Anatolide-Tauride platform with the Sakarya-Pontide terrain as evidenced by post-collisional granitoids and fission track (FT) exhumation ages of the Kırşehir block.

this time are accretion complexes along the Pontide margin metamorphosed around 100 Ma (Okay et al., 2006) and active magmatism in the Pontides beginning in the Turonian Stage (~90 Ma) and lasting through early Paleocene time (Yılmaz et al., 1997). It is important to note that the oldest age of SSZ ophiolites (179 (±15) Ma) pre-date the oldest foredeep deposits (~135 Ma) against the continent, suggesting intra-oceanic extension occurred prior to subduction against the continental margin. Thrusting and imbrication of the Eldivan SSZ basin in the central İAESZ occurred between 105 and 143 Ma as shown by detrital zircons in this study. In the western İAEO, thrusting began at least by 94 Ma, as evidence by age of a metamorphic sole (Önen, 2003). This constrains a destructive phase of subduction that began around 179 (±15) Ma and ended as early as ~60 Ma.

Final closure of the İAEO is occurred through continental block collision and suturing of the Kırşehir block and larger Anatolide-Tauride platform with the Sakarya-Pontide terrains during the Late Cretaceous period to Miocene epoch. First evidence of continental collision comes from post-collisional granitoids of the Kırşehir block that yield ages from 110 (±14) Ma (Güleç, 1994) to 74.9 (±3.8) Ma (Boztuğ et al., 2007) by Rb-Sr whole rock and ^{207}Pb-^{206}Pb zircon ages, respectively. Exhumation of the collision zone in the Central Pontides, based on stratigraphic constraints, and granitoids of the Kırşehir block, based on apatite fission track, document collision between 86-93 Ma and

57-62 Ma, respectively (Okay et al., 2006; Boztuğ and Jonckheere, 2007). Collisional indentation of the Kırşehir block caused a 33° rotation of the suture zone on the western edge of the Çankırı basin that lasted until mid-Miocene time. Ages documenting collision and suturing are younger for the central part of the suture zone where the Kırşehir block is present. In the western part of the suture where the Kırşehir block is absent and collision of the Sakayra-Pontide terrain occurred only with the Anatolide-Tauride block, exhumation is documented at 48 (±12) Ma by an $^{40}Ar/^{39}Ar$ metamorphic resetting age (Önen, 2003). This suggests the collision of the Kırşehir block with the Central Pontides may have occurred significantly earlier than collision between the Anatolide-Tauride block with the rest of the continental margin. Age for the end of collision between the Kırşehir block and Anatolide-Tauride platform with the Sakarya-Pontide terrain ended is not constrained. Boztuğ and Jonckheere (2007) attribute a second phase of granitoid exhumation in the Kırşehir block at 28-30 Ma to collision of the Arabian-African platform in the east, where Fayon et al., (2001) interpret exhumation of granitoids at 35 Ma to be from collision of the Anatolide-Tauride platform. Additional data from the İAESZ and Arabian-African platform is needed to resolve this discrepancy.

Evolution of the Eldivan ophiolite

The Eldivan ophiolite was created in the upper plate of the İAEO during oblique intra-oceanic subduction as part of a back-arc basin. This created a suite of geochemical signatures, as SSZ melting modified an N-MORB mantle and also mixed with enriched OIB mantle that had previously created seamounts on the ocean floor (Fig. 12b). We suggest the current Philippine Sea plate and Mariana SSZ basin as a modern analogue for the Eldivan ophiolite and İAEO. The Philippine Sea plate formed as an upper-plate SSZ

basin due to intra-oceanic subduction. Later, the Philippine Sea SSZ ocean basin began to subduct to the west, creating the Japan and Ryukyu arcs. In a similar way, formation of the Eldivan intra-oceanic basin began before subduction beneath the Pontides, creating the Pontide magmatic arc. Subduction of the SSZ basin beneath the Pontides caused imbrication of the ophiolite between 105 and 143 Ma (Fig 11b) and mélange development. Eventually the subduction zone was choked by collision of the Kırşehir block with the Sakarya-Pontide terrain, which further imbricated the ophiolite with the overlying Karadağ Formation. Collision continued to indent the continental margin and rotate the Eldivan ophiolite from its original NE-SW orientation to its current position.

CONCLUSION

1. The Eldivan ophiolite is a remnant of the İAEO branch of the northern Neo-Tethys that evolved as a SSZ upper plate basin between the Gondwana-derived Kirsehir and Anatolide-Tauride blocks and the Sakarya-Pontide margin.

2. Age of the Eldivan ophiolite is younger than 143 (± 2) Ma, with imbrication and initial destruction of the ocean basin occurring between 143 (± 2) Ma and 105 (± 5) Ma. This is younger than the age of imbrication of the İAEO in the west, which is documented at about 94 Ma.

3. Intra-oceanic volcanic arcs or seamounts are likely source terrains of the Eldivan ophiolite, again suggesting it formed in an intra-oceanic subduction zone away from significant continental influence.

4. This intra-oceanic subduction zone may have been oblique to the Sakarya-Pontide margin, creating a back or intra-arc spreading ridge also oblique to the continental margin with a strike of about 222, roughly NE-SW.

5. The tectonic setting and evolutionary history of the Eldivan ophiolite matches that of other Cretaceous age ophiolites of the Eastern Mediterranean, and fits well within the framework of the Tethyan Ocean system.

6. This study suggests suture zones are not a simple single subduction-collision event. They may represent multiple subduction and deformation phases and can involve several continental blocks, causing diachronous collision along strike.

REFERENCES

Akyurek, B., Bilginer, E., Catal, E., Dager, Z., Soysal, Y., & Sunu, O., 1980, Eldivan-Sabanozu (Çankırı) ve Hasayaz- Çandır (Kalecik-Ankara) dolayinin jeolojisi (the geology of Eldivan-Sabanozu (Çankırı) and Hasayaz-Candir (Kalecik-Ankara) surroundings): MTA report no: 6741 (non-published, in Turkish).

Augé, T., and Johan, Z., 1988, Comparative study of chromite deposits from Troodos, Vourinos, and North Oman and New Caledonia ophiolites, *in* Boissonas, J., and Omenetto, P. eds., Mineral Deposits within the European Community: Springer-Verlag Berlin Heidelberg.

Bailey, E.B., and McCallien, W.J., 1950, The Ankara Mélange and the Anatolian Thrust: Bulletin of Mineral Research and Exploration, Turkey, v. 40, p. 17-22.

Boztuğ, D., and Jonckheere, R.C., 2007, Apatite fission track data from central Anatolian granitoids (Turkey): Constraints on Neo-Tethyan closure: Tectonics, doi: 10.1029/2006TC001988.

Boztuğ, D., Tichomirowa, M., Bombach, K., 2007, $^{207}Pb-^{206}Pb$ single-zircon evaporation ages of some granitoids rocks reveal continent-oceanic island arc collision during the Cretaceous geodynamic evolution of the central Anatolian crust, Turkey: Journal of Asian Earth Sciences, v. 31, p. 71-86.

Bonatii, E., and Micheal, P.J., 1989, Mantle peridotites from continental rift zones to ocean basins to subduction zones. Earth and Planetary Science Letters: v. 91, p. 297-311.

Bragin, N.Y., and Tekin, U.K., 1996, Age of radiolarian-chert blacks from the Senonian Ophiolitic Mélange (Ankara, Turkey): Island Arc, v. 5, p. 114-122.

Cabanis, B., Lecolle, M., 1989, Le diagramme La/10-Y/15-Nb/8; un outil pour la discrimination des series volcaniques et la mise en evidence des processus de melange et/ou de contamination crustale. The La/10-Y/15-Nb/8 diagram; a tool for distinguishing volcanic series and discovering crustal mixing and/or contamination: Comptes Rendus de l'Academie des Sciences, Series 2, v. 309, p. 2023-2029.

Carter, J.L., 1970, Mineralogy and chemistry of the Earth's upper mantle based in the partial fusion-partial crystallization model: Geological Society of America Bulletin, v, 81, p. 2021-2034.

Çapan, U.Z., and Floyd, P.A., 1985, Geochemical and petrographic features of metabasalts within units of the Ankara Mélange, Turkey: Ofioliti, v. 10, p. 3-18.

Dick, H.J.B., Bullen, T., 1984, Chromian spinel as a petrogenetic indicator in abyssal and alpine-type peridotites and spatially associated lavas: Contributions to Mineralogy and Petrology, v. 86, p. 54-76.

Dickinson, W.R., Beard, L.S., Brakenridge, G.R., Erjavec, J.L., Ferguson, R.C., Inman, K.F., Knepp, R.A., Lindber, F.A., Byberg, P.T., 1983, Provenance of North American Phanerozoic sandstones in relation to tectonic setting: Geological Society of America Bulletin, v. 94, p. 222-235.

Dilek, Y., and Thy, P., 2006, Age and petrogenesis of plagiogranite intrusions in the Ankara, mélange, central Turkey: Island Arc, v. 15, p. 44-57.

Dril, S.I., Kuzmin, M.I., Tsipukova, S.S., Zonenshain, L.P., 1997: Geochemistry of basalts from Woodlark, Lau and Manus basins: implications for their petrogenesis and source rock compositions: Marine Geology, v. 142, p. 57-83.

Eissen, J-P., Nohara, M., Cotten, J., Hirose, K., 1994, North Fiji basin basalts and their magma source: Part I incompatible element constraints: Marine Geology, v. 116, p. 153-178.

Fayon, A.K., Whitney, D.L., Teyssier, C., Garver, J.I., Dilek, Y., 2001, Effects of plate convergence obliquity on timing and mechanisms of exhumation of a mid-crustal terrain, the Central Anatolian Crystalline Complex: Earth and Planetary Science Letters, v. 192, p. 191-205.
Fisher, R.L, and Engel. C.G., 1969, Ultramafic and basaltic rocks dredged from the nearshore flank of the Tonga trench: Geological Society of America Bulletin, v. 80, p. 137-1378.

Floyd, P. A., Kelling, G., Gökçen, S. L., Gökçen, N. 1991, Geochemistry and tectonic environment of basaltic rocks from the Misis ophiolitic mélange, south Turkey: Chemical Geology, v. 89, p.263–80.

Floyd, P.A. 1993, Geochemical discrimination and petrogenesis of alkalic basalt sequences in part of the Ankara mélange, central Turkey: Journal of the Geological Society, London, v. 150, p. 541-550.

Floyd, P.A., Yalınız, M.K., Göncüoğlu, M.C., 1998, Geochemistry and petrogenesis of intrusive and extrusive ophiolitic plagiogranites, Central Anatolian Crystalline Complex, Turkey: Lithos, v. 42, p. 225-241.

Floyd, P.A., Göncüoğlu, M.C., Winchester, J.A., Yalınız, M.K., 2000, Geochemical character and tectonic environment of Neotethyan ophiolitic fragments and metabasites in the Central Anatolian Crystalline Complex, Turkey, In: Bozkurt, E., Winchester, J.A., Piper, J.D.A., eds., Tectonics and Magmatism in Turkey and the surrounding area: Geological Society of London Special Publication, 173, p. 183-202.

Fretzdorff, S., Livermore, R.A., Devey, C.W., Leat, P.T., Stoffers, P., 2002, Petrogenesis of the back-arc East Scotia ridge, south Atlantic ocean: Journal of Petrology, v. 43, p. 1435-1467.

Frey, F., and Prinz, M., 1978, Ultramafic inclusions from San Carlos, Arizona: Petrologic and geochemical data bearing on their petrogenesis: Earth and Planetary Science Letters, v. 38, p. 129-176.

Gehrels, G., 2000, Introduction to detrital zircon studies of Paleozoic and Triassic strata in western Nevada and northern California: Geological Society of America Special Publication, v. 347, p. 1-17.

Gehrels, G., Valencia, V., Pullen, A., 2006, Detrital zircon geochronology by laser-ablation multicollector ICPMS at the Arizona LaserChron Center: Paleontological Society Papers, v. 12, p. 67-76.

Göncüoğlu, M.C., Yalınız, M.K., Tekin, U.K., 2006, Geochemistry, tectono-magmatic discrimination and radiolarian ages of basic extrusives within the İzmir -Ankara suture belt (NW Turkey): Time constraints for the Neotethyan evolution: Ofioliti, v. 31, p. 25-38.

Güleç, N., 1994, Rb–Sr isotope data from the Ağaçören granitoid (east of Tuz Gölü): geochronological and genetical implications: Turkish Journal of Earth Science, v. 3, p. 39-43.

Hakyemez, Y., Barkurt, M.Y., Bilginer, E., Pehlivan, S., Can, B., Dager, Z. and Sozeri, B. 1986, Yapraklı-Ilgaz-Çankırı-Çandır dolayinin jeolojisi: MTA report no: 7966 (non-published, in Turkish).

Harris, R.A., 1992, Peri-collisional extension and the formation of Oman-type ophiolites in the Banda Arc and Brooks Range: Geological Society Special Publications, v. 60 p. 301-325.

Harris, R.A., 1995, Geochemistry and tectonomagmatic affinity of the Misheguk massif, Brooks Range ophiolite, Alaska: Lithos, v. 35, p. 1-25.

Hawkins, J.W., and Melchior, J.T., 1985, Petrology of Mariana trough and Lau basin basalts: Journal of Geophysical Research, v. 90, p. 11,431-11,468.

Ishii, T., Robinson, P.T., Maekawa, H., Fiske, R., 1992, Petrological studies of peridotites from diapiric serpentinites seamounts in the Izu-Ogasawara-Mariana forearc, Leg 125: Proceedings of the Ocean Drilling Program, Scientific Results, v. 125, p. 445-485.

Ishii, T., 1985, Dredged samples from the Ogasawara fore-arc seamount or "Ogasawara Paleoland"-"fore-arc ophiolite, *in* Nasu, N., ed., Formation of Active Ocean Margins: Tokyo, Terra Scientific Publishing Company, p. 3307-342.
Kamenetsky, V.S., Crawford, A.J., Meffre, S., 2001, Factors controlling chemistry of magmatic spinel: and empirical study of associated olivine, Cr-spinel, and melt inclusions from primitive rocks: Journal of Petrology, v. 42, p. 655-671.

Kaymakci, N., Duermeijer, C.E., Langereis, C., White, S.H., Van Dijk, P.M., 2003, Paleomagnetic evolution of the Çankırı basin (central Anatolia, Turkey): implications for oroclinal bending due to indentation: Geological Magazine, v. 3, p. 343-355.

Koçyiğit, A., 1991, An example of an accretionary forearc basin from northern Central Anatolia and its implications for the history of Neo-Tethys in Turkey: Geological society of America Bulletin, v. 103, p. 22-36.

Kröner, A., and Şengor, A.M.C., 1990, Archean and Proterozoic ancestry in late Precambrian to early Paleozoic crustal elements of southern Turkey as revealed by single zircon dating: Geology, v. 18, p. 186-1190.

Li, Z-X. A., and Lee, C-Y. A., 2006, Geochemical investigation of serpentinized ocean lithospheric mantle in the Feather River Ophiolite, California: Implications for the recycling rate of water by subduction: Chemical Geology, v. 235, p. 161-185.

Ludwig, K.J., 2003, Isoplot 3.00: Berkeley Geochronology Center Special Publication, no. 4, 70p.

McDonough, W.F., and Sun. S.-S., 1995, The composition of the Earth: Chemical Geology, v. 120, p. 223-253.

Meschede, J.N., and Casey, J.F., 1986, A method of discriminating between different types of mid-ocean-ride basalts and continental tholeiites with the Nb-Zr-Y diagram: Chemical Geology, v. 56, p. 207-218.

Morishita, T., Maeda, J., Miyashita, S., Kumagai, H. Matsumoto, T., Dick, H.J.B., 2007, Petrology of local concentration of chromian spinel in dunite from the slow-spreading Southwest Indian Ridge: European Journal of Mineralogy, v. 19, p. 871-882.

Mullen, E.D., 1983, MnO/TiO2/P2O5: a major element discriminant for basaltic rocks of oceanic environments and its implications for petrogenesis: Earth and Planetary Science letters, v. 62, p. 53-62.

Norman, T.N., 1984, The role of the Ankara mélange in the development of Anatolia (Turkey), *in* Dixon, J.E., Robertson, A.H.F., eds., The Geological Evolution of the Eastern Mediterranean: Geological Society of London Special Publication, 17, p.441-447.

Okay, A.I. and Tüysüz, O., 1999, Tethyan sutures of northern Turkey, *in* Durand,B., Jolivet, L., Horvath, F., and Seranne, M., eds., The Mediterranean basins: Tertiary extension within the Alpine orogen: Geological Society of London Special Publication, v. 156, p. 475-515.

Okay, A.I., Tüysüz, O., Satır, M., Ozkan-Altıner, S., Altıner, D., Sherlock, S., Eren, R.H., 2006, Cretaceous and Triassic subduction-accretion, high-pressure-low-temperature metamorphism, and continental growth in the Central Pontides, Turkey: Geological Society of America Bulletin, v. 118, p. 1247-1269.

Önen, A.P., 2003, Neotethyan ophiolitic rocks of the Anatolides of NW Turkey and comparison with Tauride ophiolites: Journal of the Geological Society of London, v. 160, p. 947-962.

Paulick, H. Bach, W. Godard, M., De Hoog, J.C.M., Suhr, G., Harvey, J., 2006, Geochemistry of abyssal peridotites (Mid-Atlantic Ridge, 15º20'N, ODP leg 209): Implications for fluid/rock interaction in slow spreading environments: Chemical Geology, v. 234, p. 179-210.

Pearce, J.A., 1982, Trace element characteristics of lavas from destructive plate boundaries, *in* Thorpe, R.S., ed., Andesites: Orogenic andesites and related rocks, J. Wiley & Sons, Chichester, p. 525-548.

Pearce, J.A., Alabaster, T., Shelton, A.W., Searle, M.P., 1981, The Oman ophiolite as a Cretaceous are-basin complex: evidence and implications: Philosophical Transactions of the Royal Society of London, v. A300, p. 299-317.

Pearce, J.A., and Cann, J.R. 1973, Tectonic setting of basic volcanic rocks determined using trace element analyses: Earth and Planetary Science Letters, v. 19, p. 290-300.

Pearce, J.A., and Cann., J.R., 1971, Ophiolitic origin investigated by discriminant analysis using Ti, Zr, and Y: Earth and Planetary Science Letters, v. 12, p. 339-349.

Pearce, J.A., Harris, N.B.W., Tindle, A.G., 1984a, Trace element discrimination diagrams for the tectonic interpretation of granitic rocks: Journal of Petrology, v. 25, p. 956-983.

Pearce, J.A., Lippard, S.J., Roberts, S., 1984b, Characteristics and tectonic significance of supra-subduction zone ophiolites, *in* Kokellar, B.P., and Howells, M.F. eds., Marginal Basin Geology: Special Publication of the Geological Society of London, Blackwell Scientific Publications, Oxford, p. 77-94.

Pearce, J.A., and Norry, M.J., 1979, Petrogenetic implications of Ti, Zr, Y, and Nb variations in volcanic rocks: Contributions to Mineralogy and Petrology, v. 69, p. 33-47.

Price, R.C., Johnson, L.E., Crawford, A.J., 1990, Basalts of the North Fiji basin: the generation of back-arc basin magmas by mixing of depleted and enriched mantle sources: Contributions to mineralogy and petrology, v. 105, p. 106-121.

Rojay, B. Yalınız, K.M., Altıner, D., 2001, Tectonic implications of some cretaceous pillow basalts from the North Anatolian ophiolitic mélange (Central Anatolia-Turkey) to the evolution of Neotethys: Turkish Journal of Earth Sciences, v. 10, p. 93-102.

Rojay, B., Altıner, D., Altıner, S.O., Önen, A.P., James, S., Thirlwall, M.F., 2004, Geodynamic significance of the Cretaceous pillow basalts from North Anatolian Ophiolitic Melange Belt (Central Anatolia, Turkey): geochemical and paleontological constraints: Geodinamica Acta, v. 17, p. 349-361.

Sarıfakıoğlu, E., Özen, H., Winchester, J.A., (in press), Whole rock and mineral chemistry of ultramafic-mafic cumulates from the Orhaneli (Bursa) ophiolite, NW Anatolia: Turkish Journal of Earth Sciences, in press.

Sarıfakıoğlu, E., 2006, Petrology and origin of plagiogranites from the Daşkuplu (Eskişehir) ophiolite along the Izmir-Ankara-Erzincan suture zone, Turkey: Ofioliti, v. 32, p. 39-51.

Seifert, K., and Brunotte, D., 1996, Geochemistry of serpentinized mantle peridotite from site 897 in the Iberia abyssal plain: Proceedings of the Ocean Drilling Program, Scientific results, v. 149. p. 413-424.

Şengor, A., and Yilmaz, Y., 1981, Tethyan evolution of Turkey: A plate tectonic approach: Tectonophysics, v., 75, p. 181-241.

Shervais, J.W., 1982, Ti-V plots and petrogenesis and of modern and ophiolitic lavas: Earth and Planetary Science Letters, v. 59, p. 101-118.

Shibata, T., and Thompson, G., 1986, Peridotites from the Mid-Atlantic Ridge at 43°N and their petrogenetic relation to abyssal tholeiites: Contributions to Mineralogy and Petrology, v. 93, p. 144-159.

Sinton, J.M., and Fryer, P., 1978, Mariana lavas from 18ºN: implications fro the origin of back-arc basin basalts: Journal of Geophysical Research, v. 92, p. 12,782-12,802.

Sinton, J.M., Ford, L.L., Chappell, B., McCulloch, M.T., 2003, Magma genesis and mantle heterogeneity in the Manus back-arc basin, Papua New Guinea: Journal of Petrology, v. 44, p. 159-195.

Stacey, J.S., and Kramers, J.D., 1975, Approximation of terrestrial lead isotope evolution by a two-stage model: Earth and Planetary Science Letters, v. 26, p. 207-221.

Stern, R.J., Lin, P-N., Morris, J.D., Jackson, M.C., Fryer, P., Bloomer, S.H., Ito, E., 1990, Enriched bas-arc basin basalts from the northern Mariana Trough: implications for the evolution of back-arc basins: Earth and Planetary Science Letters, v. 100, p. 210-225.

Sun, S.-S., and McDonough, W.F., 1989, Chemical and isotopic systematics of oceanic basalts: implications for mantle composition and processes, *in* Saunders, A.D., and Norry, M.J., eds., Magmatism in the Ocean Basins: Geological Society of London Special Publication, v. 42, p. 313-345.

Takazawa, E., Okayasu, T., Satoh, K., 2003, Geochemistry and origin of the basal lherzolites from the northern Oman ophiolite (northern Fizh block): Geochemistry, Geophysics, Geosystems, v. 4, p. 1-31.

Tamura, A. Arai, S., 2006, Harzburgite-dunite-orthopyroxenite suite as a record of supra-subduction zone setting for the Oman ophiolite mantle: Lithos, v. 90, p. 43-56.

Tankut, A., 1984, Basic and ultrabasic rocks from the Ankara mélange, Turkey, i*n* Dixon, J.E., Robertson, A.H.F. eds., The Geological Evolution of the Eastern Mediterranean: Geological Society of London Special Publication, 17, p. 449-454.

Tankut, A., Dilek, Y., Önen, P., 1998, Petrology and geochemistry of the Neo-Tethyan volcanism as revealed in the Ankara mélange, Turkey: Journal of Volcanology and Geothermal Research, v. 85, p. 265-284.

Tekin, U.K., Göncüoğlu, M.C., Turhan, N., 2002, First evidence of Late Carnian radiolarians from the İzmir-Ankara suture complex, central Sakarya, Turkey: implications for the opening age of the İzmir - Ankara branch of Neo-Tethys: Geobios, v. 35, p. 127-135.

Tüysüz, O., Dellaloğu, A., Terzioğlu, N., 1995, A magmatic belt within the Neo-Tethyan suture zone and its role in the tectonic evolution of northern Turkey: Tectonophysics, v. 243, p. 173-191.

Tüysüz, O., and Tekin, U.K., 2007, Timing of imbrication of an active continental margin facing the northern branch of Neotethys, Kargı Massif, northern Turkey: Cretaceous Research v. 28, p. 754-764.

Whitney, D.L., Teyssier, C., Dilek, Y., Fayon, A.K., 2001, Metamorphism of the Central Anatolian Crystalline Complex, Turkey: influence of orogen-normal collision vs. wrench dominated tectonics on P-T-T paths: Journal of Metamorphic Geology, v. 19, p. 411-432.

Wood, D.A., 1980, The application of a Th-Hf-Ta diagram to problems of tectonomagmatic classification and to establishing the nature of crustal contamination of basaltic lavas of the British Tertiary volcanic province: Earth and Planetary Science Letters, v. 50, p. 11-30.

Woodhead, J., Eggins, S., Gamble, J., 1993, High field strength and transitional element systematics in island arc and back-arc basin basalts: evidence for multi-phase melt extraction and a depleted mantle wedge: Earth and Planetary Science Letters, v. 114, p. 491-504.

Yalınız, K.M., Floyd, P.A., Göncüoğlu, M.C., 1996, Supra-subduction zone ophiolites of Central Anatolia: geochemical evidence from the Sarıkarıman Ophiolite, Aksarya, Turkey: Mineralogical Magazine, v. 60, p. 697-710.

Yalınız, K.M, Aydin, N.S., Göncüoğlu, M.C., Parlak, O., 1999, Terlemez quartz monzonite of Central Anatolia (Arksaray-Sarıkarıman): age, petrogenesis and geotectonic implications for ophiolite emplacement: Geological Journal, v. 34, p. 233-242.

Yalınız, K.M., Floyd, P.A., Göncüoğlu, C., 2000a, Geochemistry of volcanic rocks from the Çiçekdağ Ophiolite, Central Anatolia, Turkey, and their inferred tectonic setting within the northern branch of the Neotethyan Ocean, *in* Bozkurt, E., Winchester, J.A., Piper, J.D.A., eds., Tectonics and Magmatism in Turkey and the surrounding area: Geological Society of London Special Publication, 173, p. 203-218.

Yalınız, K.M., Göncüoğlu, M.C., Ozkan- Altıner, S., 2000b, Formation and emplacement ages of the SSZ-type Neotethyan ophiolites in Central Anatolia, Turkey: palaeotectonic implications: Geological Journal, v. 35, p. 53-68.

Yılmaz, Y., Tüysüz, O., Yiğitbaş, E., Genç, S.C., Şengor, A.M.C., 1997, Geology and Tectonic evolution of the Pontides, *in* Robinson, A.G.,ed., Regional and Petroleum Geology of the Black Sea and the surrounding region: American Association of Petroleum Geologists Memoir, v. 68, p. 183-226.

APPENDIX

Table A1a. Eldivan ophiolite whole-rock geochemistry

Sample	131	265	266	270	103	110	126a	250	257	267	292c	295	296a	297b	2	3	4	5a	5b	10	11	88	220	272	274
		Peridotite			Massive Gabbro										Basalt										
SiO2	45.01	43.42	45.52	44.78	48.97	52.65	59.70	54.57	54.24	53.59	54.45	53.26	46.22	54.67	54.62	52.91	52.17	45.45	46.64	47.72	44.59	66.10	47.53	49.51	48.21
TiO2	0.02	0.06	0.02	0.01	0.50	0.75	0.25	0.33	0.33	0.46	0.93	0.97	0.71	0.91	3.01	1.49	2.22	5.05	4.38	5.05	6.42	1.21	1.20	2.01	2.02
Al2O3	1.79	2.45	1.53	0.78	17.92	18.00	11.67	17.47	17.63	16.62	15.48	16.08	16.49	15.84	12.23	15.87	13.99	11.50	12.66	11.22	10.84	13.41	15.60	14.02	14.82
Fe2O3	8.46	9.03	8.70	8.75	11.19	10.32	6.35	8.96	8.78	9.01	11.16	11.06	10.88	11.08	12.11	12.11	12.68	19.57	18.43	16.95	20.69	7.14	10.25	13.06	11.16
MnO	0.12	0.15	0.12	0.11	0.18	0.13	0.22	0.14	0.17	0.17	0.24	0.26	0.17	0.11	0.27	0.26	0.20	0.39	0.26	0.24	0.23	0.15	0.22	0.20	0.14
MgO	42.20	42.23	42.55	43.35	9.24	5.73	8.48	5.95	5.80	7.18	6.42	6.05	6.17	6.20	4.95	4.41	5.85	4.62	4.24	5.41	4.86	2.43	14.15	7.75	5.28
CaO	0.18	0.06	0.14	0.10	9.06	5.41	6.89	10.62	10.65	8.72	5.76	5.08	19.88	5.05	7.23	7.23	8.47	8.19	7.97	7.78	7.50	2.71	6.52	10.23	11.42
Na2O	0.00	0.00	0.00	0.00	2.11	4.61	4.99	1.95	1.96	3.22	5.41	5.32	0.57	5.31	5.31	5.94	4.13	3.18	3.40	3.33	2.80	5.44	2.98	3.57	4.87
K2O	0.04	0.00	0.00	0.00	1.22	1.03	0.11	0.13	0.13	1.45	0.12	0.03	0.02	0.45	0.16	0.56	0.27	0.68	0.83	0.58	0.71	0.19	0.11	0.17	1.03
P2O5	0.01	0.01	0.00	0.00	0.02	0.04	0.03	0.03	0.03	0.02	0.05	0.04	0.08	0.06	0.15	0.18	0.26	0.35	0.40	0.08	0.19	0.17	0.09	0.16	0.41
Total	97.82	97.40	98.58	97.89	100.41	98.66	98.70	100.14	99.74	100.43	100.03	98.14	101.21	99.67	100.02	100.96	100.25	98.97	99.21	98.35	98.82	98.95	98.65	100.68	99.35
ppm																									
Ni	1960	2170	2160	2210	33	26	41	33	35	127	24	31	24	23	85	63	58	23	18	19	20	<5	85	115	34
V	9.0	<5	<5	<5	445	659	133	224	226	277	449	419	383	386	339	255	266	510	348	619	1160	75	214	370	264
Cr	2450	3230	2820	3740	20	<10	180	120	120	120	20	80	30	20	<10	250	10	<10	<10	<10	<10	<10	140	360	50
Cu	21	8	15	5	43	<5	<5	20	21	12	84	<5	132	65	18	80	35	31	42	64	63	46	<5	84	64
Zn	47	65	49	45	65	49	44	42	45	62	119	80	77	107	71	125	122	216	193	176	182	100	74	124	128
Rb	1.1	0.2	0.2	0.4	16.0	10.2	0.7	2.4	2.6	18.2	1.2	0.5	0.4	2.4	2.0	15.8	4.8	14.8	18.9	22.5	31.1	2.3	1.6	1.6	5.2
Sr	0.7	1.4	4.2	13.1	141.5	139.5	39.8	134.5	140	501	67.4	52.8	46.7	71.1	110	553	143	230	279	129.5	144	210	161.5	341	73.6
Y	0.5	1.6	0.6	<0.5	7.8	10.3	9.4	7.8	7.9	10.8	19.5	20.9	15.9	19.8	83.4	51.0	69.0	43.8	46.2	41.7	46.6	33.5	24.1	19.2	33.4
Zr	5	<2	<2	<2	26	29	42	27	21	14	44	47	44	46	219	91	418	64	55	99	112	78	80	97	123
Nb	<0.2	<0.2	<0.2	<0.2	1.0	0.6	0.8	1.0	1.1	0.5	1.5	1.8	1.1	1.5	5.7	3.9	3.9	4.4	4.0	3.9	3.9	2.3	3.7	13.1	4.8
Cs	0.4	0.1	0.1	0.0	0.3	0.3	0.2	0.1	0.2	0.3	0.1	0.0	0.2	0.1	0.1	0.4	0.3	0.1	0.1	0.5	0.7	0.4	0.4	0.2	0.0
Ba	4.4	3.7	20.4	4.9	111.5	80.8	9.2	121.5	121.5	150	28.3	6.0	7.5	66.8	21.7	68.3	28.4	39.7	46.7	20.7	30.6	72.3	58.6	52.4	183.5
La	<0.5	<0.5	<0.5	<0.5	0.9	1.0	2.4	0.5	0.6	0.5	2.5	2.8	2.1	2.4	7.7	5.0	8.2	2.5	2.9	2.2	3.8	3.1	3.7	12.0	13.7
Ce	<0.5	<0.5	<0.5	<0.5	3.0	3.1	7.0	2.4	2.3	2.3	6.5	7.0	5.6	6.5	26.9	13.2	27.2	9.9	11.2	9.3	13.1	9.9	10.4	25.5	29.3
Pr	<0.03	<0.03	<0.03	<0.03	0.4	0.4	0.9	0.3	0.3	0.4	1.0	1.1	0.9	1.1	4.4	2.1	4.3	1.9	2.1	1.6	2.3	1.7	1.6	3.4	4.0
Nd	<0.1	0.1	0.1	0.1	2.0	2.0	3.9	1.6	1.6	2.3	5.3	5.6	4.5	5.4	23.7	11.3	22.4	11.6	12.9	9.7	13.3	8.9	8.1	15.0	17.7
Sm	<0.03	0.1	0.0	0.0	0.7	0.7	1.1	0.6	0.6	0.9	1.9	2.0	1.5	1.9	8.7	3.8	7.7	4.7	5.1	3.9	4.7	3.1	2.8	3.8	4.6
Eu	<0.03	0.1	<0.03	<0.03	0.3	0.3	0.5	0.3	0.3	0.6	0.8	0.8	0.6	0.8	2.2	1.5	2.9	2.2	2.3	1.5	1.8	1.2	1.0	1.5	1.5
Gd	<0.05	0.1	0.1	<0.05	0.9	1.0	1.3	0.9	0.9	1.4	2.5	2.7	2.0	2.5	10.5	5.4	9.3	6.2	6.7	4.9	6.3	4.0	3.3	4.1	5.2
Tb	<0.01	0.0	<0.01	<0.01	0.2	0.2	0.2	0.2	0.2	0.3	0.5	0.5	0.4	0.5	2.2	1.1	1.8	1.3	1.2	1.0	1.2	0.8	0.6	0.7	1.0
Dy	0.1	0.3	0.1	0.1	1.2	1.7	1.5	1.3	1.2	1.9	3.6	3.7	2.8	3.5	14.3	7.2	11.5	7.8	8.2	7.0	8.2	5.3	4.0	4.0	6.1
Ho	0.0	0.1	0.0	0.0	0.3	0.4	0.3	0.3	0.3	0.5	0.8	0.8	0.6	0.8	3.0	1.6	2.5	1.7	1.7	1.5	1.8	1.2	0.9	0.8	1.3
Er	0.1	0.2	0.1	0.0	0.9	1.1	1.0	0.9	0.8	1.3	2.3	2.5	1.9	2.3	8.7	4.4	7.1	4.6	4.8	4.5	4.8	3.4	2.4	2.0	3.8
Yb	0.1	0.2	0.1	0.1	0.9	1.2	1.0	1.0	0.9	1.4	2.3	2.4	1.8	2.4	8.3	3.9	6.7	4.2	4.2	4.5	4.5	3.2	2.4	1.7	3.7
Lu	0.0	0.0	0.0	0.0	0.1	0.2	0.2	0.2	0.2	0.2	0.4	0.4	0.3	0.4	1.3	0.6	1.1	0.7	0.6	0.6	0.7	0.5	0.3	0.3	0.6
Hf	0.2	0.2	<0.2	<0.2	0.9	1.1	1.5	0.9	0.8	0.5	1.5	1.6	1.4	1.6	6.4	2.8	10.7	2.2	1.9	3.0	3.3	2.4	2.4	2.9	3.8
Ta	<0.1	<0.1	<0.1	<0.1	0.1	0.1	0.1	0.1	0.2	0.1	0.2	0.2	0.1	0.2	0.5	0.3	0.3	0.4	0.3	0.3	0.3	0.2	0.3	1.1	0.5

Table A1b. Eldivan ophiolite whole-rock geochemistry

Sample	16	19	20	21	142	114	120	126b	127	128	129	203	210	212	215	248	293	293c	293d	280	282
	Alkaline Basalt					Sheeted Dykes											Rhyolitic rocks				
SiO2	47.77	49.47	50.32	50.05		57.37	54.75	46.65	54.54	52.99	53.21	57.00	53.77	57.97	59.02	74.90	73.57	72.68	71.79	70.55	64.40
TiO2	2.31	2.51	2.44	2.35		0.40	1.56	0.71	1.69	1.01	0.76	0.69	1.06	0.86	1.47	0.29	0.80	0.85	0.83	0.65	0.84
Al2O3	12.65	13.67	13.57	13.38		13.27	14.58	16.80	14.72	16.14	15.94	14.85	15.87	15.48	15.59	11.97	11.28	11.07	11.55	11.91	13.96
Fe2O3	11.60	11.57	10.40	11.40		9.05	13.35	8.66	14.02	10.50	9.84	8.18	11.54	10.88	11.05	4.45	5.41	5.03	6.32	5.62	8.25
MnO	0.15	0.17	0.22	0.12		0.20	0.23	0.08	0.29	0.16	0.14	0.18	0.16	0.21	0.16	0.00	0.08	0.08	0.09	0.12	0.27
MgO	11.06	7.58	6.85	6.70		7.35	4.50	5.39	4.55	6.08	7.78	5.62	7.76	5.43	2.65	0.45	1.22	1.33	1.29	1.96	3.00
CaO	9.11	8.16	7.99	8.24		5.76	6.20	22.27	5.00	8.91	6.78	6.91	4.15	3.79	5.72	0.87	1.65	1.31	1.89	4.04	4.78
Na2O	2.09	3.50	3.52	3.13		5.75	4.79	0.46	4.76	3.98	4.33	6.13	5.16	5.86	3.77	5.64	4.94	4.82	4.64	3.40	4.94
K2O	2.37	2.12	2.51	3.02		0.12	0.21	0.12	0.31	0.05	0.59	0.20	0.07	0.08	0.44	0.24	0.38	0.47	0.63	1.59	0.17
P2O5	0.31	0.31	0.30	0.27		0.05	0.12	0.08	0.14	0.08	0.05	0.07	0.05	0.04	0.20	0.04	0.15	0.18	0.17	0.10	0.12
Total	99.41	99.06	98.12	98.65	0.00	99.30	100.28	101.21	100.01	99.89	99.41	99.83	99.59	100.59	100.05	98.85	99.48	97.82	99.20	99.95	100.73
ppm																					
Ni	164	64	57	68	100	88	<5	38	<5	34	47	29	23	15	<5	<5	<5	<5	<5	18	18
V	242	271	263	268	221	247	402	311	417	231	269	245	287	325	147	14	20	48	40	183	240
Cr	330	40	40	70	210	270	<10	40	<10	100	60	20	20	10	<10	<10	<10	<10	<10	30	20
Cu	86	107	98	93	66	<5	8	343	5	40	51	12	27	10	27	8	5	<5	<5	48	44
Zn	114	130	124	133	134	50	92	42	100	75	85	62	73	36	115	30	101	98	97	84	118
Rb	38.4	32.3	40.0	45.9	14.3	0.5	2.8	1.1	3.9	0.2	4.8	1.5	0.6	0.4	4.0	1.6	8.0	9.9	14.9	45.9	3.8
Sr	466	715	575	512	502	25.9	45.3	43.7	58.1	165.5	193	116.0	90.2	52.9	193	77	87.3	128.5	121	71.4	76.1
Y	23.0	24.0	23.9	22.3	24.6	31.5	23.2	17.7	23.6	24.3	16.9	19.1	22.7	19.4	40.9	34.4	35.7	31.9	36.5	26.3	26.0
Zr	196	182	187	163	214	29	60	48	61	91	37	60	48	39	135	191	158	164	159	96	84
Nb	48.1	41.6	41.4	36.4	55.2	1.4	1.6	1.8	1.8	1.4	1.1	3.7	1.6	0.9	4.3	4.9	3.9	3.9	3.8	4.6	2.5
Cs	0.1	0.8	0.1	0.1	0.5	0.0	0.1	0.2	0.1	0.0	0.2	0.1	0.1	0.0	0.2	0.1	0.2	0.5	0.7	1.9	0.3
Ba	610	1105	952	1130	339	8.4	18.7	5.1	23.9	7.7	65.7	17.5	10.8	16.8	75.6	17.7	26.8	37.9	39.9	123	37.6
La	37.7	31.5	32.0	28.7	42.7	2.1	2.7	2.3	2.6	2.7	1.7	4.8	2.1	1.1	6.8	6.5	7.3	4.7	5.7	12.9	6.7
Ce	74.2	63.2	64.9	57.4	81.4	6.8	7.9	6.7	8.0	8.9	5.4	10.7	6.9	3.9	18.7	15.9	20.7	14.1	16.9	27.5	16.3
Pr	8.2	7.3	7.2	6.6	8.5	1.1	1.2	1.0	1.2	1.4	0.8	1.3	1.0	0.6	2.7	2.3	3.3	2.4	2.8	3.6	2.3
Nd	32.3	29.0	28.9	26.5	32.6	5.9	6.4	4.6	6.5	7.3	4.2	6.1	5.6	3.3	13.8	11.5	16.3	12.8	14.4	15.4	11.0
Sm	6.3	6.2	6.1	5.7	6.3	2.6	2.3	1.5	2.1	2.6	1.5	1.8	2.1	1.5	4.6	4.0	5.0	4.3	4.8	3.9	3.3
Eu	1.9	1.9	1.9	1.8	2.0	0.4	1.0	0.6	0.9	1.1	0.6	0.7	0.7	0.5	1.6	1.5	1.9	1.5	1.7	1.2	1.1
Gd	6.3	6.1	6.0	5.6	6.3	3.4	2.9	2.2	2.9	3.1	2.0	2.4	2.5	2.2	5.6	4.6	5.9	5.2	5.7	4.3	3.6
Tb	0.9	0.9	0.9	0.8	0.9	0.7	0.6	0.4	0.6	0.6	0.4	0.4	0.5	0.5	1.1	0.9	1.2	1.0	1.1	0.8	0.7
Dy	4.4	4.7	4.7	4.3	4.6	5.2	3.8	2.9	4.0	4.1	2.8	3.0	3.5	3.1	6.9	5.8	7.1	6.3	6.9	4.8	4.7
Ho	0.9	0.9	0.9	0.8	0.9	1.1	0.8	0.6	0.9	0.9	0.6	0.7	0.8	0.7	1.5	1.2	1.5	1.3	1.5	1.1	1.1
Er	2.2	2.4	2.4	2.2	2.2	3.5	2.4	1.8	2.6	2.5	1.8	1.9	2.5	2.0	4.4	3.7	4.1	3.7	4.3	3.0	3.2
Yb	1.8	1.9	1.7	1.8	1.9	3.9	2.3	1.8	2.4	2.6	1.8	2.0	2.6	2.2	4.2	3.9	3.9	3.1	4.3	3.0	3.3
Lu	0.3	0.3	0.3	0.3	0.3	0.6	0.3	0.3	0.4	0.4	0.3	0.3	0.4	0.3	0.7	0.6	0.6	0.4	0.7	0.5	0.5
Hf	5.1	4.7	4.8	4.4	5.0	1.2	1.9	1.6	2.1	2.6	1.3	1.7	1.7	1.5	4.0	5.8	4.7	5.0	4.9	3.0	2.8
Ta	3.0	2.5	2.6	2.3	3.5	0.1	0.1	0.1	0.2	0.1	0.1	0.3	0.1	0.1	0.4	0.5	0.5	0.5	0.5	0.5	0.2

Table A2a. Peridotite Cr-spinel mineral chemistry

Sample	270	270	270	271	271	271	271	271	271	271	271	271	271	271	271	271	271	271	271	271
SiO2	0.07	0.03	0.13	0.07	0.11	0.06	0.20	0.07	0.08	0.05	0.06	0.04	0.11	0.06	0.01	0.02	0.06	0.05	0.04	0.01
TiO2	0.01	0.01	0.02	0.31	0.48	0.39	0.19	0.22	0.14	0.13	0.32	0.23	0.15	0.00	0.03	0.00	0.00	0.02	0.01	0.03
Al2O3	25.02	28.34	27.23	18.47	21.13	21.29	20.17	18.13	24.74	24.04	17.70	22.63	17.64	22.41	23.92	19.45	20.58	21.69	21.97	22.83
Cr2O3	45.64	43.88	43.49	51.73	49.77	49.86	50.97	52.63	47.41	47.86	52.49	49.28	51.27	47.93	46.06	50.34	49.47	48.46	47.20	47.62
FeO	13.96	14.60	15.28	16.64	14.77	14.99	17.02	17.14	13.15	13.97	15.86	13.90	12.65	16.24	14.79	15.91	15.96	14.79	15.29	13.22
Fe2O3	1.72	0.00	0.00	0.51	0.00	0.73	0.00	0.18	0.34	0.00	1.70	0.67	4.18	0.00	1.38	1.20	0.20	0.97	1.59	0.99
NiO	0.10	0.13	0.00	0.00	0.16	0.15	0.10	0.16	0.08	0.17	0.04	0.00	0.09	0.14	0.07	0.02	0.02	0.07	0.06	0.08
MnO	0.49	0.47	0.47	0.64	0.52	0.50	0.57	0.58	0.52	0.57	0.64	0.54	0.63	0.59	0.56	0.60	0.63	0.61	0.53	0.55
MgO	14.33	13.75	13.19	11.77	13.42	13.52	10.94	11.45	14.91	13.46	12.41	14.31	14.32	12.11	13.43	12.07	12.00	13.05	12.73	14.21
Total	101.32	101.21	99.81	100.13	100.35	101.48	100.17	100.56	101.36	100.23	101.22	101.58	101.04	99.48	100.25	99.60	98.91	99.70	99.41	99.54
FeO*	13.37	12.84	12.33	11.22	12.59	12.67	10.41	10.89	13.93	12.68	11.80	13.41	13.51	11.48	12.64	11.46	11.42	12.35	11.98	13.33
Calculated on 32 oxygens																				
Si	0.02	0.01	0.03	0.02	0.03	0.01	0.05	0.02	0.02	0.01	0.02	0.01	0.03	0.01	0.00	0.01	0.02	0.01	0.01	0.00
Ti	0.00	0.00	0.00	0.06	0.09	0.07	0.04	0.04	0.03	0.02	0.06	0.04	0.03	0.00	0.01	0.00	0.00	0.00	0.00	0.01
Al	7.04	7.89	7.73	5.48	6.12	6.10	5.95	5.38	6.94	6.87	5.20	6.42	5.13	6.56	6.86	5.76	6.10	6.32	6.43	6.58
Cr	8.62	8.20	8.28	10.29	9.67	9.59	10.08	10.47	8.92	9.18	10.34	9.37	10.00	9.41	8.86	10.01	9.84	9.47	9.26	9.21
Fe2+	2.79	2.89	3.08	3.50	3.03	3.05	3.56	3.61	2.62	2.84	3.31	2.80	2.61	3.37	3.01	3.35	3.36	3.06	3.17	2.71
Fe3+	0.31	0.00	0.00	0.10	0.00	0.13	0.00	0.03	0.06	0.00	0.32	0.12	0.78	0.00	0.25	0.23	0.04	0.18	0.30	0.18
Ni	0.02	0.03	0.00	0.00	0.03	0.03	0.02	0.03	0.02	0.03	0.01	0.00	0.02	0.03	0.01	0.00	0.00	0.01	0.01	0.02
Mn	0.10	0.09	0.10	0.14	0.11	0.10	0.12	0.12	0.10	0.12	0.13	0.11	0.13	0.12	0.12	0.13	0.13	0.13	0.11	0.11
Mg	5.10	4.85	4.74	4.41	4.92	4.90	4.08	4.30	5.29	4.87	4.61	5.13	5.27	4.49	4.87	4.52	4.50	4.81	4.71	5.18
Cr# [Cr/(Cr+Al)]	0.55	0.51	0.52	0.65	0.61	0.61	0.63	0.66	0.56	0.57	0.67	0.59	0.66	0.59	0.56	0.63	0.62	0.60	0.59	0.58
Mg# [Mg/(Mg/Fe2+)]	0.65	0.63	0.61	0.56	0.62	0.62	0.53	0.54	0.67	0.63	0.58	0.65	0.67	0.57	0.62	0.57	0.57	0.61	0.60	0.66

Sample	271	271	271	271	271	271	271	271	271	271	271	850	850	850	850	850	850	850	850	850
SiO2	1.24	0.06	0.01	0.05	0.03	0.02	0.02	0.00	0.06	0.04	0.06	0.01	0.03	0.00	0.02	0.00	0.02	0.03	0.04	0.02
TiO2	0.02	0.01	0.01	0.03	0.04	0.03	0.02	0.03	0.04	0.02	0.04	0.04	0.04	0.03	0.04	0.02	0.05	0.06	0.02	0.05
Al2O3	22.82	20.00	24.34	24.04	23.97	24.16	24.47	24.78	23.35	23.89	24.65	17.37	17.25	17.55	16.29	15.73	15.47	16.13	16.81	16.19
Cr2O3	45.18	50.11	46.74	47.06	46.18	45.97	46.07	45.55	47.51	46.47	46.11	49.55	49.91	49.33	51.34	52.22	52.48	52.06	51.30	51.73
FeO	14.51	15.83	13.30	13.79	13.98	13.95	13.73	13.75	13.34	13.19	13.24	19.55	18.91	18.71	18.13	18.17	18.18	18.42	19.15	18.76
Fe2O3	2.30	1.08	1.14	0.55	0.49	0.17	0.70	0.25	1.06	1.17	1.08	3.64	3.45	3.35	2.86	2.80	2.90	2.40	2.14	2.77
NiO	0.05	0.08	0.06	0.15	0.12	0.10	0.09	0.14	0.11	0.05	0.12	0.10	0.06	0.02	0.10	0.03	0.08	0.03	0.02	0.02
MnO	0.55	0.57	0.52	0.55	0.60	0.57	0.52	0.00	0.53	0.51	0.52	0.63	0.64	0.61	0.61	0.65	0.68	0.66	0.68	0.68
MgO	13.14	12.27	14.55	14.10	13.70	13.67	14.09	14.26	14.35	14.40	14.57	9.65	10.00	10.05	10.31	10.23	10.23	10.14	9.69	9.96
Total	99.81	100.03	100.67	100.31	99.11	98.64	99.70	98.77	100.34	99.74	100.39	100.52	100.29	99.65	99.70	99.85	100.08	99.94	99.85	100.18
FeO*	12.38	11.62	13.62	13.24	12.93	12.87	13.19	12.83	13.44	13.46	13.63	9.31	9.64	9.65	9.88	9.86	9.88	9.78	9.39	9.64
Calculated on 32 oxygens																				
Si	0.30	0.02	0.00	0.01	0.01	0.01	0.01	0.00	0.01	0.01	0.02	0.00	0.01	0.00	0.01	0.00	0.01	0.01	0.01	0.01
Ti	0.00	0.00	0.00	0.01	0.01	0.01	0.00	0.01	0.01	0.00	0.01	0.01	0.01	0.01	0.01	0.00	0.01	0.01	0.01	0.01
Al	6.56	5.88	6.90	6.86	6.93	7.00	7.00	7.13	6.67	6.84	6.99	5.24	5.20	5.32	4.95	4.79	4.70	4.90	5.11	4.91
Cr	8.71	9.89	8.89	9.01	8.95	8.94	8.85	8.80	9.10	8.92	8.77	10.03	10.10	10.02	10.46	10.66	10.70	10.60	10.46	10.53
Fe2+	2.96	3.30	2.68	2.79	2.87	2.87	2.79	2.81	2.70	2.68	2.66	4.19	4.05	4.02	3.91	3.92	3.92	3.97	4.13	4.04
Fe3+	0.42	0.20	0.21	0.10	0.09	0.03	0.13	0.05	0.19	0.21	0.20	0.70	0.66	0.65	0.56	0.54	0.56	0.47	0.42	0.54
Ni	0.01	0.02	0.01	0.03	0.02	0.02	0.02	0.03	0.02	0.01	0.02	0.02	0.01	0.00	0.02	0.01	0.02	0.01	0.00	0.00
Mn	0.11	0.12	0.11	0.11	0.13	0.12	0.11	0.00	0.11	0.10	0.11	0.14	0.14	0.13	0.13	0.14	0.15	0.14	0.15	0.15
Mg	4.78	4.57	5.22	5.09	5.01	5.01	5.10	5.19	5.18	5.21	5.23	3.68	3.82	3.85	3.96	3.94	3.93	3.90	3.72	3.82
Cr# [Cr/(Cr+Al)]	0.57	0.63	0.56	0.57	0.56	0.56	0.56	0.55	0.58	0.57	0.56	0.66	0.66	0.65	0.68	0.69	0.69	0.68	0.67	0.68
Mg# [Mg/(Mg/Fe2+)]	0.62	0.58	0.66	0.65	0.64	0.64	0.65	0.65	0.66	0.66	0.66	0.47	0.49	0.49	0.50	0.50	0.50	0.50	0.47	0.49

Table A2b. Peridotite Cr-spinel mineral chemistry

Sample	850	850	850	850	850	850	850	850	850	850	850	850	850	850	850	850	850	850	850	19
SiO2	0.04	0.01	0.02	0.01	0.03	0.01	0.04	0.05	0.02	0.00	0.02	0.03	0.08	0.01	0.23	7.58	0.03	0.01	0.00	0.06
TiO2	0.03	0.05	0.04	0.04	0.04	0.03	0.03	0.03	0.04	0.04	0.03	0.04	0.03	0.03	0.02	0.03	0.04	0.03	0.04	0.02
Al2O3	20.84	15.48	15.43	16.06	15.70	16.09	16.07	15.89	15.98	15.52	15.57	15.24	15.30	15.81	15.77	12.65	16.00	15.46	15.58	26.19
Cr2O3	46.29	53.28	53.01	52.52	52.37	52.44	52.81	52.98	52.25	53.51	53.30	53.26	52.59	53.14	52.45	43.00	52.46	52.40	52.67	45.48
FeO	19.85	18.36	18.12	18.68	18.85	17.84	17.62	17.34	17.58	17.74	17.55	17.68	17.42	17.49	17.48	7.30	17.89	18.33	18.30	13.00
Fe2O3	1.95	2.22	2.68	2.53	2.57	2.56	2.74	2.40	2.85	2.41	2.42	2.37	3.42	2.21	2.71	11.26	2.44	2.31	2.70	0.99
NiO	0.06	0.07	0.07	0.02	0.16	0.01	0.05	0.02	0.03	0.11	0.00	0.09	0.09	0.02	0.07	0.00	0.10	0.06	0.00	0.05
MnO	0.58	0.65	0.64	0.65	0.66	0.61	0.63	0.61	0.63	0.68	0.65	0.64	0.62	0.63	0.63	0.57	0.64	0.64	0.63	0.52
MgO	9.56	10.18	10.35	10.11	9.83	10.59	10.83	10.89	10.71	10.63	10.72	10.50	10.76	10.76	10.68	14.85	10.49	9.97	10.21	15.09
Total	99.19	100.29	100.36	100.62	100.21	100.18	100.81	100.21	100.09	100.62	100.25	99.84	100.30	100.10	100.05	97.24	100.09	99.22	100.13	101.39
FeO*	9.19	9.81	9.95	9.74	9.50	10.14	10.38	10.41	10.26	10.24	10.29	10.09	10.30	10.31	10.24	13.93	10.08	9.61	9.82	14.10
Calculated on 32 oxygens																				
Si	0.01	0.00	0.01	0.00	0.01	0.00	0.01	0.01	0.01	0.00	0.01	0.01	0.02	0.00	0.06	1.87	0.01	0.00	0.00	0.01
Ti	0.01	0.01	0.01	0.01	0.01	0.01	0.01	0.01	0.01	0.01	0.01	0.01	0.01	0.01	0.00	0.01	0.01	0.01	0.01	0.00
Al	6.26	4.70	4.68	4.85	4.78	4.86	4.82	4.79	4.83	4.68	4.71	4.64	4.63	4.78	4.77	3.67	4.84	4.74	4.73	7.30
Cr	9.34	10.85	10.78	10.64	10.69	10.63	10.63	10.72	10.60	10.83	10.81	10.87	10.67	10.78	10.64	8.37	10.65	10.78	10.73	8.50
Fe2+	4.24	3.95	3.90	4.00	4.07	3.83	3.75	3.71	3.77	3.80	3.76	3.82	3.74	3.75	3.75	1.50	3.84	3.99	3.94	2.57
Fe3+	0.37	0.43	0.52	0.49	0.50	0.49	0.53	0.46	0.55	0.46	0.47	0.46	0.66	0.43	0.52	2.09	0.47	0.45	0.52	0.18
Ni	0.01	0.02	0.01	0.00	0.03	0.00	0.01	0.00	0.01	0.02	0.00	0.02	0.02	0.01	0.02	0.00	0.02	0.01	0.00	0.01
Mn	0.13	0.14	0.14	0.14	0.14	0.13	0.14	0.13	0.14	0.15	0.14	0.14	0.13	0.14	0.14	0.12	0.14	0.14	0.14	0.10
Mg	3.64	3.91	3.97	3.86	3.78	4.05	4.11	4.16	4.10	4.06	4.10	4.04	4.12	4.11	4.09	5.45	4.02	3.87	3.92	5.32
Cr# [Cr/(Cr+Al)]	0.60	0.70	0.70	0.69	0.69	0.69	0.69	0.69	0.69	0.70	0.70	0.70	0.70	0.69	0.69	0.70	0.69	0.69	0.69	0.54
Mg# [Mg/(Mg/Fe2+)]	0.46	0.50	0.50	0.49	0.48	0.51	0.52	0.53	0.52	0.52	0.52	0.51	0.52	0.52	0.52	0.78	0.51	0.49	0.50	0.67

Sample	19	19	19	19	19	19	19	19	19	19	19	19	19	19	19	19	19	19	19	19
SiO2	0.01	0.76	0.03	0.04	0.05	0.39	0.13	0.04	0.06	0.08	0.07	0.03	0.04	0.02	0.04	0.07	0.06	0.04	0.03	0.06
TiO2	0.03	0.01	0.01	0.01	0.00	0.02	0.00	0.01	0.02	0.02	0.03	0.00	0.02	0.03	0.00	0.01	0.00	0.02	0.02	0.02
Al2O3	26.91	20.75	26.76	26.97	26.85	30.48	27.64	26.17	28.77	27.60	27.61	27.26	27.26	27.63	26.14	26.03	26.91	27.74	27.50	26.57
Cr2O3	44.48	34.08	44.82	44.45	44.51	40.30	43.55	45.10	41.94	43.84	44.41	43.82	44.43	44.18	45.03	45.02	44.71	43.85	44.07	44.71
FeO	12.88	15.56	12.94	12.67	12.18	12.87	12.86	13.21	12.81	12.12	12.53	12.78	12.18	11.73	12.82	12.89	12.39	11.28	11.56	13.42
Fe2O3	0.46	16.83	0.49	0.91	0.86	0.80	0.91	1.01	0.88	0.99	0.87	0.79	0.87	0.67	1.16	0.77	0.96	1.09	0.82	1.01
NiO	0.07	0.07	0.08	0.05	0.19	0.11	0.03	0.09	0.12	0.09	0.12	0.06	0.12	0.11	0.12	0.09	0.07	0.09	0.19	0.08
MnO	0.51	0.49	0.50	0.50	0.52	0.54	0.54	0.54	0.55	0.52	0.50	0.51	0.50	0.48	0.55	0.52	0.51	0.50	0.50	0.53
MgO	15.06	12.48	15.06	15.30	15.51	15.43	15.18	14.85	15.24	15.71	15.62	15.14	15.68	15.98	15.06	14.91	15.50	16.27	16.01	14.80
Total	100.41	101.02	100.68	100.90	100.66	100.94	100.85	101.02	100.41	100.96	101.74	100.37	101.09	100.82	100.91	100.30	101.12	100.88	100.70	100.91
FeO*	14.06	11.72	14.04	14.26	14.47	14.43	14.21	13.90	14.27	14.65	14.56	14.12	14.61	14.85	14.11	13.93	14.46	15.15	14.91	13.85
Calculated on 32 oxygens																				
Si	0.00	0.19	0.01	0.01	0.01	0.09	0.03	0.01	0.01	0.02	0.02	0.01	0.01	0.01	0.01	0.02	0.02	0.01	0.01	0.01
Ti	0.01	0.00	0.00	0.00	0.00	0.00	0.00	0.00	0.00	0.00	0.01	0.00	0.00	0.00	0.00	0.00	0.00	0.00	0.00	0.00
Al	7.54	6.03	7.48	7.51	7.49	8.35	7.68	7.33	7.99	7.65	7.61	7.62	7.56	7.65	7.32	7.33	7.48	7.66	7.63	7.42
Cr	8.36	6.65	8.41	8.31	8.33	7.40	8.12	8.47	7.82	8.15	8.21	8.22	8.26	8.21	8.46	8.50	8.33	8.12	8.20	8.37
Fe2+	2.56	3.21	2.57	2.50	2.41	2.50	2.54	2.63	2.53	2.38	2.45	2.54	2.40	2.31	2.55	2.58	2.44	2.21	2.28	2.66
Fe3+	0.08	3.12	0.09	0.16	0.15	0.14	0.16	0.18	0.16	0.18	0.15	0.14	0.15	0.12	0.21	0.14	0.17	0.19	0.15	0.18
Ni	0.01	0.01	0.02	0.01	0.04	0.02	0.01	0.02	0.02	0.02	0.02	0.01	0.02	0.02	0.02	0.02	0.01	0.02	0.04	0.02
Mn	0.10	0.10	0.10	0.10	0.10	0.11	0.11	0.11	0.11	0.10	0.10	0.10	0.10	0.10	0.11	0.10	0.10	0.10	0.10	0.11
Mg	5.34	4.59	5.33	5.39	5.47	5.35	5.34	5.26	5.36	5.51	5.44	5.36	5.50	5.60	5.33	5.31	5.45	5.68	5.62	5.23
Cr# [Cr/(Cr+Al)]	0.53	0.52	0.53	0.53	0.53	0.47	0.51	0.54	0.49	0.52	0.52	0.52	0.52	0.52	0.54	0.54	0.53	0.51	0.52	0.53
Mg# [Mg/(Mg/Fe2+)]	0.68	0.59	0.67	0.68	0.69	0.68	0.68	0.67	0.68	0.70	0.69	0.68	0.70	0.71	0.68	0.67	0.69	0.72	0.71	0.66

Table A3a. U-Pb Detrital zircon geochronology. Regular type- 35 micron spot analysis, bold type- 25 micron spot analysis.

				Isotope ratios							Apparent ages (Ma)					
#	U	206Pb	U/Th	206Pb*	±	207Pb*	±	206Pb*	±	error	206Pb*	±	207Pb*	±	206Pb*	±
	(ppm)	204Pb		207Pb*	(%)	235U*	(%)	238U	(%)	corr.	238U*	(Ma)	235U	(Ma)	207Pb*	(Ma)
Sample AD012 Karadag Fm																
2	66	1136	1.0	17.2828	30.1	0.1573	30.2	0.0197	2.5	0.08	125.8	3.1	148.3	41.7	524.5	673.3
3	52	828	1.0	16.1761	36.6	0.1598	36.8	0.0188	3.5	0.10	119.8	4.2	150.6	51.5	667.8	809.1
4	51	804	1.0	24.4570	22.2	0.1155	22.2	0.0205	1.0	0.05	130.7	1.3	111.0	23.3	-294.6	571.8
5	95	1228	0.7	25.1848	21.4	0.1122	21.5	0.0205	1.7	0.08	130.8	2.2	108.0	22.0	-370.0	560.3
6	79	980	1.0	22.6647	17.4	0.1246	17.5	0.0205	1.9	0.11	130.7	2.5	119.3	19.7	-103.9	430.8
7	472	10136	1.5	17.6135	6.7	0.5104	7.1	0.0652	2.4	0.33	407.2	9.3	418.7	24.5	482.8	148.9
8	552	10496	1.2	20.5296	1.8	0.1557	2.4	0.0232	1.7	0.69	147.8	2.4	147.0	3.3	133.9	41.5
9	128	7416	1.8	18.3564	3.8	0.5382	4.7	0.0717	2.8	0.60	446.1	12.2	437.2	16.8	390.8	84.9
10	83	2284	2.1	20.4875	10.5	0.1664	10.7	0.0247	1.7	0.16	157.4	2.6	156.3	15.5	138.7	248.2
11	67	1092	1.0	22.7613	10.4	0.1223	11.4	0.0202	4.5	0.40	128.8	5.7	117.1	12.6	-114.4	257.4
12	55	876	1.2	22.6311	28.1	0.1225	28.3	0.0201	2.9	0.10	128.3	3.7	117.3	31.3	-100.3	702.3
13	97	1596	0.8	21.3839	12.3	0.1303	12.4	0.0202	1.8	0.14	129.0	2.3	124.4	14.5	37.2	294.7
14	1159	15476	1.7	20.1553	1.7	0.1603	3.0	0.0234	2.5	0.82	149.3	3.6	151.0	4.2	177.0	40.1
15	67	872	1.1	17.1830	45.8	0.1496	45.9	0.0186	3.6	0.08	119.1	4.2	141.6	60.8	537.2	1055.6
17	42	1064	1.5	20.7232	40.4	0.1425	40.4	0.0214	2.3	0.06	136.6	3.1	135.3	51.3	111.8	989.3
18	221	2936	0.5	21.0379	4.7	0.1327	4.9	0.0203	1.4	0.29	129.3	1.8	126.5	5.8	76.1	110.7
19	56	876	1.0	25.6751	23.3	0.1106	23.4	0.0206	1.2	0.05	131.4	1.6	106.5	23.6	-420.2	617.7
20	51	660	1.2	20.4148	27.5	0.1441	27.6	0.0213	2.2	0.08	136.1	2.9	136.7	35.3	147.0	655.9
21	124	1524	0.4	22.4847	18.8	0.1197	19.0	0.0195	3.0	0.16	124.6	3.7	114.8	20.7	-84.3	463.7
22	120	1456	0.6	20.0308	13.7	0.1416	13.8	0.0206	1.4	0.10	131.3	1.8	134.5	17.4	191.4	321.1
23	70	1404	1.1	18.7970	17.6	0.1400	18.1	0.0191	4.1	0.23	121.9	4.9	133.0	22.6	337.3	402.1
24	63	408	0.9	18.9393	11.9	0.1494	12.3	0.0205	3.2	0.26	130.9	4.1	141.3	16.2	320.2	270.2
25	57	760	0.8	19.0061	11.8	0.1500	11.9	0.0207	1.8	0.15	131.9	2.4	141.9	15.8	312.2	269.3
27	237	2708	0.6	18.5119	10.9	0.1533	11.1	0.0206	1.6	0.14	131.3	2.0	144.8	14.9	371.8	247.1
28	162	2108	0.7	23.0425	12.1	0.1309	12.2	0.0219	1.3	0.11	139.5	1.8	124.9	14.3	-144.8	300.4
29	89	712	0.7	15.2699	23.2	0.1991	23.2	0.0220	1.3	0.06	140.6	1.8	184.3	39.1	790.0	492.1
31	64	772	1.0	30.8811	36.0	0.0913	36.2	0.0205	3.3	0.09	130.5	4.2	88.7	30.7	-930.1	1078.9
32	141	2804	0.9	21.8494	8.2	0.1559	8.6	0.0247	2.6	0.30	157.3	4.0	147.1	11.8	-14.6	199.6
33	323	2560	0.4	17.1379	18.9	0.1636	18.9	0.0203	1.0	0.05	129.8	1.3	153.9	27.0	542.9	416.0
35	98	680	0.7	14.9228	17.9	0.2048	18.0	0.0222	1.5	0.08	141.3	2.1	189.2	31.0	838.1	375.3
36	155	1856	0.8	21.1470	7.9	0.1265	8.3	0.0194	2.5	0.30	123.9	3.1	121.0	9.4	63.8	188.1
37	246	2292	0.6	20.9586	5.7	0.1339	6.2	0.0204	2.5	0.40	129.9	3.2	127.6	7.4	85.0	134.5
38	174	3116	1.2	21.3721	8.7	0.1361	8.8	0.0211	1.4	0.16	134.5	1.9	129.5	10.7	38.5	208.5
39	65	996	0.9	20.3217	15.7	0.1338	16.7	0.0197	5.9	0.35	125.9	7.4	127.5	20.1	157.7	368.2
10	57	932	0.9	21.4935	31.1	0.1322	31.2	0.0206	1.4	0.04	131.5	1.8	126.0	36.9	24.9	762.7
41	82	1256	0.9	20.8703	16.7	0.1351	16.8	0.0204	1.4	0.08	130.5	1.8	128.7	20.3	95.1	397.9
42	52	756	0.8	23.2365	27.7	0.1196	28.2	0.0201	4.8	0.17	128.6	6.1	114.7	30.5	-165.5	701.8
43	70	1028	0.8	27.4376	27.9	0.0992	28.2	0.0197	4.1	0.15	126.0	5.1	96.0	25.8	-597.3	769.6
44	67	1048	0.8	19.8264	32.6	0.1408	32.7	0.0202	2.4	0.07	129.2	3.0	133.7	41.0	215.2	774.2
45	128	1864	0.8	22.9935	12.2	0.1206	12.5	0.0201	2.8	0.23	128.3	3.6	115.6	13.6	-139.4	301.9
46	186	3592	1.1	20.2601	8.8	0.1743	9.0	0.0256	1.8	0.19	163.0	2.8	163.2	13.6	164.8	206.7
47	43	484	1.4	20.3063	35.6	0.1121	35.6	0.0165	1.2	0.03	105.6	1.3	107.9	36.5	159.5	857.1
48	499	4048	0.4	20.9745	3.5	0.1383	3.8	0.0210	1.6	0.41	134.2	2.1	131.5	4.7	83.2	83.0
49	93	1448	0.6	26.8236	29.7	0.1141	29.7	0.0222	1.1	0.04	141.5	1.6	109.7	30.9	-536.2	809.9
50	79	784	1.0	17.9530	21.1	0.1537	21.2	0.0200	2.5	0.12	127.7	3.2	145.2	28.7	440.4	474.0
51	49	712	1.0	23.9027	16.6	0.1237	16.7	0.0214	1.6	0.10	136.7	2.2	118.4	18.6	-236.4	420.9
52	268	3716	0.5	20.8364	4.4	0.1540	4.7	0.0233	1.7	0.36	148.3	2.4	145.4	6.3	98.9	103.1

Table A3b. U-Pb Detrital zircon geochronology. Regular type- 35 micron spot analysis, bold type- 25 micron spot analysis.

				Isotope ratios							Apparent ages (Ma)					
#	U	206Pb	U/Th	206Pb*	±	207Pb*	±	206Pb*	±	error	206Pb*	±	207Pb*	±	206Pb*	±
	(ppm)	204Pb		207Pb*	(%)	235U*	(%)	238U	(%)	corr.	238U*	(Ma)	235U	(Ma)	207Pb*	(Ma)
Sample AD012 Karadag Fm																
53	588	4528	0.3	19.2872	12.3	0.1343	13.1	0.0188	4.6	0.35	119.9	5.5	127.9	15.8	278.7	282.4
54	76	508	1.2	19.6078	63.0	0.1493	63.4	0.0212	7.6	0.12	135.5	10.2	141.3	83.9	240.8	1615.1
55	200	4080	1.1	20.6207	7.3	0.1746	7.3	0.0261	1.0	0.14	166.1	1.6	163.4	11.1	123.5	171.6
57	377	2436	1.2	21.1660	5.0	0.1760	5.4	0.0270	2.1	0.38	171.9	3.5	164.6	8.2	61.6	119.3
59	113	984	1.0	21.0459	13.6	0.1414	13.7	0.0216	1.2	0.09	137.6	1.6	134.3	17.2	75.2	324.9
60	75	1040	0.9	25.9392	22.6	0.1039	23.2	0.0195	5.2	0.22	124.8	6.4	100.4	22.2	-447.1	602.5
61	66	1084	1.0	25.4259	21.7	0.1038	21.9	0.0191	2.8	0.13	122.3	3.4	100.3	20.9	-394.8	571.6
62	77	1060	0.9	22.5195	11.8	0.1284	12.3	0.0210	3.4	0.28	133.8	4.5	122.6	14.2	-88.1	290.1
63	1509	12208	1.4	20.2377	5.4	0.1627	5.5	0.0239	1.0	0.19	152.1	1.5	153.1	7.9	167.4	127.0
64	1789	3204	1.5	16.8013	16.3	0.1951	16.4	0.0238	1.4	0.08	151.5	2.0	181.0	27.1	586.1	355.9
65	68	472	0.8	22.6108	28.7	0.1226	28.8	0.0201	2.3	0.08	128.3	2.9	117.4	32.0	-98.1	718.3
25-1	**75**	**330**	**0.7**	**22.9893**	**35.5**	**0.1131**	**35.7**	**0.0189**	**3.4**	**0.10**	**120.5**	**4.1**	**108.8**	**36.8**	**-139.0**	**903.7**
25-2	**58**	**549**	**1.0**	**18.0383**	**16.8**	**0.1617**	**16.9**	**0.0212**	**2.3**	**0.13**	**135.0**	**3.0**	**152.2**	**24.0**	**429.9**	**376.6**
25-3	**59**	**735**	**0.7**	**15.7366**	**37.7**	**0.1880**	**37.8**	**0.0215**	**2.2**	**0.06**	**136.9**	**3.0**	**174.9**	**60.7**	**726.5**	**827.5**
25-4	**131**	**960**	**1.1**	**17.4696**	**24.2**	**0.1472**	**24.5**	**0.0186**	**3.6**	**0.15**	**119.1**	**4.2**	**139.4**	**31.9**	**500.9**	**540.6**
25-5	**1731**	**4161**	**0.5**	**20.3773**	**3.4**	**0.1685**	**3.8**	**0.0249**	**1.7**	**0.44**	**158.5**	**2.7**	**158.1**	**5.6**	**151.4**	**80.8**
25-6	**188**	**2292**	**1.1**	**22.6023**	**10.0**	**0.1276**	**10.2**	**0.0209**	**1.6**	**0.16**	**133.5**	**2.1**	**121.9**	**11.7**	**-97.2**	**246.8**
25-7	**279**	**2790**	**0.9**	**20.1748**	**8.4**	**0.1428**	**8.8**	**0.0209**	**2.6**	**0.30**	**133.3**	**3.5**	**135.5**	**11.1**	**174.7**	**195.2**
25-8	**699**	**6546**	**2.0**	**20.7225**	**8.1**	**0.1063**	**8.8**	**0.0160**	**3.5**	**0.39**	**102.2**	**3.5**	**102.6**	**8.6**	**111.8**	**192.3**
25-9	**929**	**8340**	**1.4**	**20.7391**	**1.8**	**0.1115**	**2.9**	**0.0168**	**2.3**	**0.78**	**107.2**	**2.4**	**107.4**	**2.9**	**110.0**	**42.9**
25-10	**731**	**6039**	**1.6**	**18.2844**	**24.8**	**0.1207**	**24.9**	**0.0160**	**2.5**	**0.10**	**102.3**	**2.5**	**115.7**	**27.3**	**399.6**	**563.6**
25-11	**485**	**4314**	**2.2**	**19.7491**	**4.3**	**0.1910**	**4.5**	**0.0274**	**1.5**	**0.33**	**174.0**	**2.6**	**177.5**	**7.3**	**224.2**	**98.4**
25-12	**132**	**963**	**0.5**	**18.4186**	**11.5**	**0.1344**	**12.0**	**0.0180**	**3.3**	**0.27**	**114.7**	**3.7**	**128.1**	**14.4**	**383.2**	**260.1**
25-13	**133**	**6114**	**1.5**	**12.1793**	**3.2**	**1.9907**	**4.0**	**0.1758**	**2.5**	**0.62**	**1044.2**	**23.8**	**1112.4**	**27.1**	**1248.0**	**61.9**
25-14	**1066**	**10971**	**1.6**	**14.0484**	**12.5**	**0.2483**	**12.5**	**0.0253**	**1.0**	**0.08**	**161.0**	**1.6**	**225.2**	**25.3**	**962.6**	**256.0**
25-15	**105**	**912**	**0.7**	**15.4967**	**15.3**	**0.1683**	**16.5**	**0.0189**	**6.3**	**0.38**	**120.8**	**7.6**	**157.9**	**24.2**	**759.0**	**324.1**
25-15a	**63**	**747**	**1.1**	**21.8308**	**19.7**	**0.1467**	**19.8**	**0.0232**	**1.3**	**0.06**	**148.0**	**1.9**	**139.0**	**25.7**	**-12.5**	**480.2**
25-16	**202**	**2004**	**0.8**	**13.8938**	**8.2**	**0.2047**	**8.3**	**0.0206**	**1.0**	**0.12**	**131.6**	**1.3**	**189.1**	**14.2**	**985.2**	**167.0**
25-17	**111**	**486**	**0.5**	**21.0250**	**25.6**	**0.1306**	**25.8**	**0.0199**	**3.3**	**0.13**	**127.1**	**4.1**	**124.7**	**30.3**	**77.5**	**617.9**
25-18	**148**	**1488**	**1.0**	**18.5027**	**7.9**	**0.1503**	**8.0**	**0.0202**	**1.6**	**0.20**	**128.7**	**2.1**	**142.2**	**10.6**	**373.0**	**177.2**
25-20	**68**	**1149**	**0.9**	**16.7655**	**24.4**	**0.1545**	**24.8**	**0.0188**	**4.3**	**0.17**	**120.0**	**5.1**	**145.9**	**33.7**	**590.7**	**536.8**
Sample AD009 Ophiolitic Melange																
1	112	42955	4.0	12.7606	1.0	2.0815	1.7	0.1926	1.4	0.81	1135.7	14.5	1142.7	11.7	1156.2	19.8
2	505	20945	1.2	20.0645	1.0	0.1680	2.0	0.0244	1.8	0.87	155.7	2.7	157.7	3.0	187.5	23.3
3	233	24905	2.7	19.6550	2.9	0.3295	3.6	0.0470	2.1	0.59	295.9	6.1	289.2	9.1	235.3	67.2
4	97	5005	1.3	20.8711	8.3	0.1529	8.4	0.0231	1.7	0.20	147.5	2.5	144.5	11.4	95.0	196.2
5	344	23360	2.1	19.6607	4.7	0.2734	5.1	0.0390	2.0	0.39	246.5	4.7	245.4	11.1	234.6	108.3
6	201	9185	1.5	19.4428	6.2	0.1716	6.3	0.0242	1.0	0.16	154.2	1.5	160.8	9.4	260.3	143.6
7	272	9275	0.9	21.0865	3.9	0.1508	5.0	0.0231	3.0	0.61	147.0	4.4	142.6	6.6	70.6	93.1
8	711	28700	1.0	20.5243	3.2	0.1704	3.4	0.0254	1.0	0.30	161.4	1.6	159.7	5.0	134.5	76.0
9	113	5540	2.2	21.5410	9.4	0.1518	9.5	0.0237	1.3	0.13	151.1	1.9	143.5	12.7	19.6	226.5
10	175	12395	1.3	21.3972	6.8	0.1548	6.9	0.0240	1.2	0.17	153.0	1.8	146.2	9.4	35.7	162.3
11	110	5920	1.3	21.0325	11.5	0.1570	11.9	0.0239	2.9	0.24	152.6	4.4	148.1	16.4	76.7	274.7
12	525	10380	1.1	21.0241	4.1	0.1533	4.4	0.0234	1.7	0.38	149.0	2.5	144.8	6.0	77.6	97.5
13	109	5445	1.5	19.7789	7.8	0.1802	7.8	0.0258	1.0	0.13	164.5	1.6	168.2	12.2	220.7	180.2
15	177	72730	3.0	9.9249	1.0	3.9799	1.4	0.2865	1.0	0.71	1623.9	14.4	1630.1	11.5	1638.1	18.6
16	481	8750	1.6	18.0945	6.3	0.1744	6.5	0.0229	1.6	0.24	145.8	2.2	163.2	9.8	423.0	140.5

Table A3c. U-Pb Detrital zircon geochronology. Regular type- 35 micron spot analysis, bold type- 25 micron spot analysis.

				Isotope ratios							Apparent ages (Ma)					
#	U	206Pb	U/Th	206Pb*	±	207Pb*	±	206Pb*	±	error	206Pb*	±	207Pb*	±	206Pb*	±
	(ppm)	204Pb		207Pb*	(%)	235U*	(%)	238U	(%)	corr.	238U*	(Ma)	235U	(Ma)	207Pb*	(Ma)
Sample AD009 Ophiolitic Melange																
17	432	13730	1.5	20.6133	4.6	0.1558	4.9	0.0233	1.7	0.34	148.4	2.4	147.0	6.6	124.3	107.6
18	124	47620	1.5	7.9033	1.0	6.2503	1.5	0.3583	1.1	0.75	1974.0	19.4	2011.5	13.3	2050.3	17.7
13	212	6110	0.9	21.2261	5.8	0.1461	5.9	0.0225	1.0	0.17	143.4	1.4	138.5	7.7	54.9	139.6
20	544	8540	1.4	18.5369	13.0	0.1632	13.1	0.0219	1.5	0.12	139.9	2.1	153.5	18.6	368.8	293.6
22	379	13920	1.5	20.3626	4.5	0.1583	4.8	0.0234	1.8	0.37	149.0	2.6	149.2	6.7	153.0	105.0
23	116	2320	1.3	14.3073	10.1	0.2300	10.2	0.0239	1.6	0.15	152.1	2.4	210.2	19.4	925.2	207.9
24	222	10605	2.1	18.0167	2.4	0.3652	3.1	0.0477	2.0	0.64	300.5	5.8	316.1	8.4	432.6	52.9
25	127	4445	1.3	19.0159	10.3	0.1742	10.5	0.0240	2.0	0.19	153.0	3.0	163.1	15.8	311.0	234.5
25-1	**256**	**636**	**2.6**	**18.8858**	**15.8**	**0.1766**	**16.1**	**0.0242**	**3.2**	**0.20**	**154.1**	**4.8**	**165.1**	**24.6**	**326.6**	**361.4**
25-2	**636**	**17583**	**2.2**	**16.0144**	**1.9**	**0.8031**	**2.3**	**0.0933**	**1.2**	**0.54**	**574.9**	**6.7**	**598.6**	**10.2**	**689.3**	**40.5**
25-3	**179**	**4185**	**1.4**	**17.0760**	**14.9**	**0.2052**	**14.9**	**0.0254**	**1.0**	**0.07**	**161.8**	**1.6**	**189.5**	**25.8**	**550.8**	**326.6**
25-4	**222**	**6018**	**1.9**	**20.6592**	**11.3**	**0.1639**	**11.4**	**0.0246**	**1.6**	**0.14**	**156.4**	**2.5**	**154.1**	**16.3**	**119.1**	**267.5**
25-5	**540**	**10473**	**1.1**	**20.4560**	**3.2**	**0.1686**	**3.4**	**0.0250**	**1.3**	**0.38**	**159.3**	**2.0**	**158.2**	**5.0**	**142.3**	**74.2**
25-6	**268**	**8841**	**1.3**	**21.2937**	**7.4**	**0.1603**	**7.9**	**0.0248**	**2.8**	**0.35**	**157.7**	**4.3**	**151.0**	**11.0**	**47.3**	**176.2**
25-7	**898**	**50112**	**1.7**	**18.2908**	**1.0**	**0.5066**	**1.4**	**0.0672**	**1.0**	**0.69**	**419.3**	**4.1**	**416.1**	**4.9**	**398.8**	**23.3**
25-8	**987**	**6642**	**1.0**	**18.5354**	**8.5**	**0.1745**	**8.7**	**0.0235**	**1.8**	**0.20**	**149.5**	**2.6**	**163.3**	**13.2**	**369.0**	**192.9**
25-9	**1067**	**1734**	**1.6**	**15.4770**	**31.7**	**0.1999**	**31.7**	**0.0224**	**1.0**	**0.03**	**143.1**	**1.4**	**185.0**	**53.7**	**761.7**	**684.9**
25-10	**168**	**630**	**0.8**	**15.4446**	**37.0**	**0.1821**	**37.2**	**0.0204**	**3.3**	**0.09**	**130.2**	**4.2**	**169.9**	**58.2**	**766.1**	**806.8**
25-11	**254**	**5991**	**1.1**	**20.6852**	**10.9**	**0.1689**	**11.0**	**0.0253**	**1.1**	**0.10**	**161.3**	**1.7**	**158.5**	**16.1**	**116.1**	**258.7**
25-11a	**239**	**8184**	**1.3**	**19.2827**	**6.8**	**0.1720**	**6.9**	**0.0241**	**1.5**	**0.22**	**153.2**	**2.3**	**161.2**	**10.3**	**279.2**	**155.2**